

SDSPT2s: SDSPT2 with Selection

Yibo Lei,^{*,†} Yang Guo,[‡] Bingbing Suo,[¶] and Wenjian Liu^{*,‡}

[†]Key Laboratory of Synthetic and Natural Functional Molecule of the Ministry of Education,
College of Chemistry and Materials Science, Shaanxi key Laboratory of Physico-Inorganic
Chemistry, Northwest University, Xi'an 710127, China

[‡]Qingdao Institute for Theoretical and Computational Sciences, School of Chemistry and
Chemical Engineering, Shandong University, Qingdao 266237, China

[¶]Institute of Modern Physics, Northwest University, and Shaanxi Key Laboratory for
Theoretical Physics Frontiers, Xi'an 710127, China

E-mail: leiya@nwu.edu.cn; liuwj@sdu.edu.cn

Abstract

As an approximation to SDSCI [static-dynamic-static (SDS) configuration interaction (CI), a minimal MRCI; *Theor. Chem. Acc.* 133, 1481 (2014)], SDSPT2 [*Mol. Phys.* 115, 2696 (2017)] is a CI-like multireference (MR) second-order perturbation theory (PT2) that treats single and multiple roots in the same manner. This feature permits the use of configuration selection over a large complete active space (CAS) P to end up with a much reduced reference space \tilde{P} , which is connected only with a small portion (\tilde{Q}_1) of the full first-order interacting space Q connected to P . The most expensive portion of the reduced interacting \tilde{Q}_1 space (which involves three active orbitals) can further be truncated by partially bypassing its generation followed by an integral-based cutoff. With marginal loss of accuracy, the selection-truncation procedure, along with an efficient evaluation and storage of internal contraction coefficients, renders SDSPT2s (SDSPT2 with selection) applicable to systems that cannot

be handled by the parent CAS-based SDSPT2, as demonstrated by several challenging showcases.

1 Introduction

A system of strongly correlated electrons is characterized by a large number of energetically adjacent and singly occupied frontier orbitals. The strong static/nondynamic correlation among such orbitals renders the many-electron wave function a heavy mixture of a huge number of Slater determinants or equivalently configuration state functions (CSF). As such, such systems (especially of low spins) go beyond the capability of single reference methods. Instead, the use of a multireference (MR) method is mandatory. The available MR methods can be classified into three families:¹ static-then-dynamic (SD), dynamic-then-static (DS), and static-dynamic-static (SDS). The SD family of methods start with a diagonalization of the bare molecular Hamiltonian projected onto a reference/active space $P = \{\Phi_R; R = [1, N_R]\}$, so as to obtain a reference state $\Psi_k^{(0)} = \sum_{R=1}^{N_R} \Phi_R \bar{C}_{Rk}^{(0)}$. This step captures static correlation, especially when $\Psi_k^{(0)}$ is only qualitatively or semi-quantitatively correct. The remaining dynamic correction to $\Psi_k^{(0)}$ can be accounted for in a number of ways, even just to first order $\Psi_k^{(1)}$. Classic examples of this family of methods include complete active space (CAS) second-order perturbation theory (CASPT2),^{2,3} multiconfiguration quasi-degenerate perturbation theory,⁴ and n-electron valence second-order perturbation theory (NEVPT2).^{5,6} A common feature of such methods lies in that the coefficients $\bar{C}_{Rk}^{(0)}$ of the reference state $\Psi_k^{(0)}$ are used to construct $\Psi_k^{(1)}$ for dynamic correlation but are not relaxed in the presence of dynamic correlation. Colloquially, dynamic correlation sees static correlation but static correlation does not see dynamic correlation. This is true even for their multi-state (MS) variants⁷⁻¹⁰ because of their insufficient revision of the coefficients $\bar{C}_{Rk}^{(0)}$. In contrast, the DS family of methods incorporate dynamic correction to each reference function Φ_R and then construct and diagonalize an effective Hamiltonian in the space P , thereby producing a wave function that can be (very) different from $\Psi_k^{(0)}$ obtained by diagonalizing the bare Hamiltonian in the same space. Classic examples are the (shifted) B_k type of methods.¹¹⁻¹⁶ Since the zero-order coefficients $\bar{C}_{Rk}^{(0)}$ are not involved in the dynamic correlation step at

all, it can be said that dynamic correlation does not see static correlation in such family of methods. It should hence be clear that both the SD and DS families of methods cannot achieve balanced treatments of the static and dynamic components of the overall correlation, especially when the two components are strongly entangled and even interchangeable. This situation warrants a SDS type of treatment, where the predetermined coefficients $\bar{C}_{Rk}^{(0)}$ are used in dynamic correlation but are then sufficiently or even fully relaxed in the presence of dynamic correlation. That is, the static and dynamic components of the overall correlation do see each other. Several variants of multireference second-order perturbation theory (MRPT2),^{17–26} internally contracted multireference configuration interaction (ic-MRCI),^{27–39} and internally contracted multireference coupled-cluster methods^{40–53} belong to this family. However, such methods usually require the construction and diagonalization of a large Hamiltonian matrix even just for one state. At variance with this, one of the present authors proposed⁵⁴ a restricted SDS framework for constructing many-electron wave functions, where no matter how many electrons and how many orbitals are to be correlated, only a $3N_p$ -by- $3N_p$ Hamiltonian matrix is constructed and diagonalized for N_p states. The framework leads to a series of methods, including SDSCI,⁵⁴ SDSPT2,⁵⁵ iterative configuration interaction (iCI),¹ iCI with configuration and perturbation (iCIPT2),^{56,57} and extended variants⁵⁸ of SDSCI and SDSPT2. Albeit a minimal MRCI, SDSCI is very close in accuracy to ic-MRCI,^{59,60} with a computational cost being only that of one iteration of ic-MRCI. As an approximation to SDSCI, SDSPT2 is a CI-like MRPT2 and treats single and multiple roots in the same way. In particular, SDSPT2 gives rise to MS-NEVPT2 for free. While SDSPT2 is usually very similar to MS-NEVPT2 in accuracy,^{59–64} it does outperform MS-NEVPT2 for situations with multiple nearly degenerate states⁵⁵. As an iterative version of SDSCI, iCI is an exact solver of full CI, whereas iCIPT2 is one of the most efficient near-exact methods.⁶⁵ Taking iCI as the CASCI solver, we obtain iCISCF,⁶⁶ which can handle active spaces as large as (60e, 60o).

One major problem associated with the above multireference methods lies in that a

large reference space P leads to an exceedingly large first-order interacting space (FOIS) Q that is intractable. The only way to go is to reduce the reference space from P to \tilde{P} , so as to reduce the FOIS from Q to \tilde{Q}_1 . The \tilde{Q}_1 space can further be treated approximately by separating it into an important subset that is treated rigorously and an unimportant subset that can be treated approximately. Several approaches have been proposed along this line,⁶⁷⁻⁷⁰ which differ from each other in the choice of reduced reference space \tilde{P} , zeroth-order Hamiltonian H_0 , perturbations spanning \tilde{Q}_1 , and effective Hamiltonian to be diagonalized for the final solutions. In the present work, we apply such approximations to the complete active space self-consistent field (CASSCF)-based SDSPT2,⁵⁵ so as to render it applicable to systems that require very large active spaces.

The paper is organized as follows. The essential features of SDSPT2⁵⁵ are first recapitulated in Sec. 2. The hole-particle symmetry-based graphic unitary group approach (HPS-GUGA)³² is then employed in Sec. 3 to generate excited configuration state functions (CSF) from individual orbital configurations (oCFG) contained in the reduced reference wave functions $\tilde{\Psi}_k^{(0)} = \sum_{R=1}^{\tilde{N}_R} \Phi_R \tilde{C}_{Rk}^{(0)}$ that result from truncation of the CASSCF/iCISCF⁶⁶ wave functions $\Psi_k^{(0)} (= \sum_R^{N_R} \Phi_R \tilde{C}_{Rk}^{(0)})$. Noticeably, many of the so-generated CSFs do not belong to the \tilde{Q}_1 space and hence have zero matrix elements with the reduced reference wave functions $\tilde{\Psi}_k^{(0)}$. As such, they should first be screened out. Moreover, those double excitations involving three active orbitals (TAOD) are computationally most expensive and will hence be screened during the construction of reduced sub-DRTs (distinct row table⁷¹) and also by an integral-based cutoff. The efficacy of the resulting SDSPT2s (SDSPT2 with selection) is illustrated in Sec. 4 with several challenging systems, including a simplified model of heme, chromium dimer, $\text{Cu}_2\text{O}_2^{2+}$ core, and cobalt nitrosyl complex $[\text{Co}(\text{TC}-3,3)(\text{NO})]$. The paper is closed with a summary in Sec. 5.

Unless otherwise stated, the notations documented in Table 1 are to be used for the

orbitals and states, under the Einstein summation convention over repeated indices.

Table 1: Notations for the orbitals and states

space	indices
orbital space	
arbitrary orbitals	p, q, r, s
hole (or closed) orbitals	i, j
active orbitals	u, v, t, w
external (or virtual) orbitals	a, b
configuration space	
step vector in HPS-GUGA	$(\mathbf{d})_\mu = [(\mathbf{d})_e(\mathbf{d})_a(\mathbf{d})_h]_\mu$
configuration state function (CSF)	Φ_μ
reference CSF	Φ_R
reference orbital configuration	$\Phi_R^o = \prod_{i=1}^n \psi_i^{n_i}; n_i \in [0, 2]$
excited CSF	Φ_q
reference wavefunction	$\Psi_k^{(0)}$
electronic state	Ψ_I
node of distinct row tableaux (DRT)	$(a_r, b_r)_I$
sub-DRT	$(\bar{X}Y)$
internally contracted configuration	$\bar{\Phi}_{Mk}^{\bar{X}Y}$
complete active space	P
full first-order interacting space (FOIS)	Q
reduced reference space	\bar{P}
reduced FOIS generated from $\{\Phi_R^o\}$ in \bar{P}	$\bar{Q} = \bar{Q}_1 + \bar{Q}_r$
reduced FOIS interacting with \bar{P}	\bar{Q}_1

2 SDSPT2

The *restricted* SDS framework⁵⁴ starts with the following wave functions for N_P lowest states

$$|\Psi_I\rangle = \sum_k^{N_P} |\Psi_k^{(0)}\rangle \tilde{C}_{kI} + \sum_k^{N_P} |\Xi_k^{(1)}\rangle \tilde{C}_{(k+N_P)I} + \sum_k^{N_P} |\Theta_k^{(2)}\rangle \tilde{C}_{(k+2N_P)I}, \quad (1)$$

where $\Psi_k^{(0)}$ ($= \sum_{R=1}^{N_R} \Phi_R \bar{C}_{Rk}^{(0)}$), $\Xi_k^{(1)}$, and $\Theta_k^{(2)}$ represent the zeroth-order, first-order, and secondary functions, respectively. By introducing the primary (P_m) and secondary (P_s)

parts of the P space,

$$P_m = \sum_{k=1}^{N_p} |\Psi_k^{(0)}\rangle\langle\Psi_k^{(0)}|, \quad (2)$$

$$P_s = P - P_m = \sum_{l=N_p+1}^{N_R} |\Psi_l^{(0)}\rangle\langle\Psi_l^{(0)}|, \quad (3)$$

the first-order ($\Xi_k^{(1)}$) and secondary ($\Theta_k^{(2)}$) functions can be defined as

$$|\Xi_k^{(1)}\rangle = Q \frac{1}{E_k^{(0)} - H_0} QH|\Psi_k^{(0)}\rangle = \sum_{q \in Q} |\Psi_{q,k}^{(0)}\rangle \bar{C}_{qk}^{(1)}, \quad (4)$$

$$Q = 1 - P = \sum_{q \in Q} |\Psi_{q,k}^{(0)}\rangle\langle\Psi_{q,k}^{(0)}|, \quad (5)$$

$$|\Theta_k^{(2)}\rangle = P_s H |\Xi_k^{(1)}\rangle \quad (6)$$

$$\approx P'_s H |\Xi_k^{(1)}\rangle, \quad P'_s = \sum_{l=N_p+1}^{N_p+M_p} |\Psi_l^{(0)}\rangle\langle\Psi_l^{(0)}|, \quad (7)$$

$$= \sum_{R \in P} |\Phi_R\rangle \bar{C}_{Rk}^{(2)}, \quad (8)$$

$$\bar{C}_{Rk}^{(2)} = \sum_{S \in P} \sum_{q \in Q} \bar{D}_{RS}^{(0)} \langle \Phi_S | H | \Psi_{q,k}^{(0)} \rangle \bar{C}_{qk}^{(1)}, \quad (9)$$

$$\bar{D}_{RS}^{(0)} = \sum_{l=N_p+1}^{N_p+M_p} \bar{C}_{Rl}^{(0)} \bar{C}_{Sl}^{(0)}, \quad R, S \in P. \quad (10)$$

Note that $\{|\Psi_{q,k}^{(0)}\rangle\}$ in Eq. (4) are eigenvectors of a zeroth-order Hamiltonian H_0 ,

$$H_0 |\Psi_{q,k}^{(0)}\rangle = E_{q,k}^{(0)} |\Psi_{q,k}^{(0)}\rangle, \quad q \in Q, \quad k \in [1, N_p], \quad (11)$$

which may be state-specific or state-collective (independent of state k). Eq. (6) represents the projection of the Lanczos vector $H|\Xi_k^{(1)}\rangle$ onto the secondary space, which is further approximated to Eq. (7) to simplify the evaluation of the matrix elements. It is clear from Eq. (8) that the secondary functions are linear combinations of the reference CSFs $\{\Phi_R\}$ but with their coefficients related to the first-order functions. As such, they can facilitate

the relaxation of the reference coefficients $\bar{C}_{Rk}^{(0)}$ in the presence of dynamic correlation, particularly for avoided crossings¹ or multiple near-degenerate states.⁵⁵ The fact that $|\Psi_k^{(0)}\rangle$, $|\Xi_k^{(1)}\rangle$, and $|\Theta_k^{(2)}\rangle$ have decreasing weights in the wave function $|\Psi_I\rangle$ justifies the characterization of them as primary, external, and secondary states. Since both $|\Xi_k^{(1)}\rangle$ and $|\Theta_k^{(2)}\rangle$ are specific to $|\Psi_k^{(0)}\rangle$, the generalized eigenvalue problem

$$\tilde{\mathbf{H}}\tilde{\mathbf{C}} = \tilde{\mathbf{S}}\tilde{\mathbf{C}}\tilde{\mathbf{E}} \quad (12)$$

for determining the expansion coefficients of $|\Psi_I\rangle$ is only of dimension $3N_p$. The Hamiltonian and metric matrices have the following structures

$$\tilde{\mathbf{H}} = \begin{pmatrix} P_m H P_m & P_m H Q & P_m H P_s \\ Q H P_m & Q H Q & Q H P_s \\ P_s H P_m & P_s H Q & P_s H P_s \end{pmatrix} \quad (13)$$

$$= \begin{pmatrix} E_k^{(0)} \delta_{kl} & \langle \Psi_k^{(0)} | H | \Xi_l^{(1)} \rangle & 0 \\ \langle \Xi_l^{(1)} | H | \Psi_k^{(0)} \rangle & \langle \Xi_k^{(1)} | H | \Xi_l^{(1)} \rangle & \langle \Xi_k^{(1)} | H | \Theta_l^{(2)} \rangle \\ 0 & \langle \Theta_l^{(2)} | H | \Xi_k^{(1)} \rangle & \langle \Theta_k^{(2)} | H | \Theta_l^{(2)} \rangle \end{pmatrix}, \quad k, l = 1, \dots, N_p, \quad (14)$$

$$\tilde{\mathbf{S}} = \begin{pmatrix} \delta_{kl} & 0 & 0 \\ 0 & \langle \Xi_k^{(1)} | \Xi_l^{(1)} \rangle & 0 \\ 0 & 0 & \langle \Theta_k^{(2)} | \Theta_l^{(2)} \rangle \end{pmatrix}. \quad (15)$$

The above is nothing but a minimal MRCI (dubbed as SDSCI⁵⁴). Taking SDSCI as the seed, various methods can be derived,^{1,56-58} among which the simplest variant is SDSPT2, which amounts to replacing the QHQ block in Eq. (13) with QH_0Q . Like NEVPT2,⁵ the

Dyall CAS/A Hamiltonian⁷² is adopted here for H_0 :

$$H_0 = H_I^D + H_A^D, \quad (16)$$

$$H_I^D = \sum_i \epsilon_i \hat{E}_{ii} + \sum_a \epsilon_a \hat{E}_{aa} + C_I^D, \quad \hat{E}_{pq} = a^{p\sigma} a_{q\sigma}, \quad (17)$$

$$H_A^D = \sum_{tu} f_{tu}^c \hat{E}_{tu} + \frac{1}{2} \sum_{tuvw} (tu|vw) \hat{e}_{tu,vw}, \quad \hat{e}_{tu,vw} = \hat{E}_{tu} \hat{E}_{vw} - \delta_{uv} \hat{E}_{tw}, \quad (18)$$

$$C_I^D = E^c - 2 \sum_i \epsilon_i, \quad E^c = \sum_i (h_{ii} + f_{ii}^c), \quad (19)$$

$$f_{pq}^c = h_{pq} + \sum_i [2(pq|ii) - (pi|i q)], \quad (20)$$

where the quasi-canonical orbital energies, ϵ_i and ϵ_a , are obtained by diagonalizing the generalized Fock matrix

$$F_{pq} = f_{pq}^c + \sum_{tu} [(pq|tu) - \frac{1}{2}(pu|tq)] D_{tu}, \quad (21)$$

$$D_{tu} = \sum_k w_k \langle \Psi_k^{(0)} | \hat{E}_{tu} | \Psi_k^{(0)} \rangle \quad (22)$$

for the doubly occupied and virtual subspaces separately. The particular choice of the constant C_I^D (19) is to make $\langle \Phi_\mu | H^D | \Phi_\nu \rangle$ equal to $\langle \Phi_\mu | H | \Phi_\nu \rangle$ for all Φ_R in P , such that

$$\langle \Psi_k^{(0)} | H^D | \Psi_l^{(0)} \rangle = \langle \Psi_k^{(0)} | H | \Psi_l^{(0)} \rangle = E_k^{(0)} \delta_{kl}, \quad (23)$$

where

$$E_k^{(0)} = E^c + \sum_{tu} f_{tu}^c \langle \Psi_k^{(0)} | \hat{E}_{tu} | \Psi_k^{(0)} \rangle + \frac{1}{2} \sum_{tuvw} (tu|vw) \langle \Psi_k^{(0)} | \hat{e}_{tu,vw} | \Psi_k^{(0)} \rangle. \quad (24)$$

Since H_0 (16) does not couple⁵⁵ different classes of excitations (cf. Table 2), Eq. (11) can be solved for each class ($K \in [1, 8]$) of excitations separately. Still, however, this is possible only when the state-specific, orthonormalized internally contracted configurations (ICC)⁶⁸ are used as the basis to expand the zeroth-order eigenvectors (perturbbers)

$|\Psi_{(qK),k}^{(0)}\rangle$ (vide post). Once this is done, the QH_0Q block in Eq. (13) can readily be constructed as

$$\langle \Xi_k^{(1)} | H_0 | \Xi_l^{(1)} \rangle = \sum_{(qK), (rK) \in Q} \bar{C}_{(qK),k}^{(1)} \langle \Psi_{(qK),k}^{(0)} | H_0 | \Psi_{(rK),l}^{(0)} \rangle \bar{C}_{(rK),l}^{(1)} \quad (25)$$

$$\approx \frac{1}{2} \sum_{(qK), (rK) \in Q} [E_{(qK),k}^{(0)} + E_{(rK),l}^{(0)}] \langle \Psi_{(qK),k}^{(0)} | \Psi_{(rK),l}^{(0)} \rangle \bar{C}_{(qK),k}^{(1)} \bar{C}_{(rK),l}^{(1)}, \quad (26)$$

$$\bar{C}_{(qK),k}^{(1)} = \frac{\langle \Psi_{(qK),k}^{(0)} | H | \Psi_k^{(0)} \rangle}{E_k^{(0)} - E_{(qK),k}^{(0)}}, \quad K \in [1, 8]. \quad (27)$$

Since the most numerous matrix elements $\langle \Psi_{(qK),k}^{(0)} | H | \Phi_R \rangle$ are shared by $\bar{C}_{(qK),k}^{(1)}$ (27), $\bar{C}_{(qK),k}^{(2)}$ (9), QHP_m/P_mHQ , and QHP_s/P_sHQ , and the other matrix elements in Eqs. (14) and (15) can readily be evaluated, SDSPT2 has little computational overhead over MS-NEVPT2 (which only requires the P_mHP_m and P_mHQ blocks). It is obvious that SDSPT2 can produce MS-NEVPT2 for free. However, it should be noted that, unlike NEVPT2, SDSPT2 is not size consistent. Nevertheless, the size consistency errors can readily be cured by the Pople correction,⁷³ as demonstrated before.⁵⁹

Table 2: Correspondence between excitation operators \hat{E}_M and sub-DRTs ($\bar{X}Y$)

Class K	\hat{E}_M	N_d^a	N_e^b	$\bar{X}Y^c$	$N_{XY}^{ex,d}$
0	$\hat{E}_{uv}, \hat{e}_{uv,tw}$	0	0	$\bar{V}V$	0
1	$\hat{E}_{ui}, \hat{e}_{ui,vw}$	1	0	$\bar{D}V$	0, 1, 2
2	$\hat{E}_{au}, \hat{e}_{au,vw}$	0	1	$\bar{V}D$	0, 1
3	$\hat{E}_{ai}, \hat{e}_{ai,uv}, \hat{e}_{ui,av}$	1	1	$\bar{D}D$	0, 1
4	$\hat{e}_{ui,vj}$	2	0	$\bar{P}V$	0, 1, 2
5	$\hat{e}_{au,bv}$	0	2	$\bar{V}P$	0
6	$\hat{e}_{ai,uj}$	2	1	$\bar{P}D$	0, 1
7	$\hat{e}_{ai,bu}$	1	2	$\bar{D}P$	0
8	$\hat{e}_{ai,bj}$	2	2	$\bar{P}P$	0

^a Number of holes in the hole space.

^b Number of electrons in the virtual space.

^c P = S or T; S: two-electron singlet; T: two-electron triplet; D: one-electron doublet; V: void.

^d Allowed excitation number of sub-DRT ($\bar{X}Y$).

3 Implementation of SDSPT2s

Even though the FOIS Q can be decomposed into 8 disjoint subspaces (see Table 2), the major computational step of the CAS-based SDSPT2⁵⁵ (and NEVPT2^{5,6,10}) is still the diagonalization of the Dyall Hamiltonian (16) to produce the perturbbers $\{\Psi_{(qK),k}^{(0)}\}$ (11). To remedy this, the SDSPT2s scheme is proposed here. The very first step is to reduce the CAS P to \tilde{P} . That is, after the iCISCF(2)⁶⁶ calculations (NB: iCISCF(2) emphasizes that the total energy is the sum of the iCISCF variational energy and second-order Epstein-Nesbet perturbation (ENPT2)^{74,75} correction within the CAS), only those CSFs with coefficients larger in absolute value than the preset threshold P_{\min} for any state are to be retained. The survival CSFs $\{\Phi_R\}_{R=1}^{\tilde{N}_R}$ span the \tilde{P} space. Although it is in principle possible to generate the interacting excited CSFs $\Phi_q \in \tilde{Q}_1$ directly from $\{\Phi_R\}_{R=1}^{\tilde{N}_R}$, it is in practice more efficient^{68,76} to obtain them by exciting the reference orbital configurations (oCFG) $\{\Phi_R^o\}_{R=1}^{N_R^o}$ contained in \tilde{P} , via the HPS-GUGA.³² A problem lies in that $\{\Phi_R^o\}_{R=1}^{N_R^o}$ are usually just a subset of those oCFGs contained in space P , such that the HPS-GUGA³² designed for a CAS reference must be modified (see Sec. 3.1). Another problem that does not occur to a CAS reference lies in that many excited CSFs $\Phi_r \in \tilde{Q}_r = \tilde{Q} - \tilde{Q}_1$ generated this way do not interact with the \tilde{P} space. Nevertheless, they can readily be eliminated by invoking the conditions $\langle \Phi_r | \hat{E}_{pq} | \Psi_k^{(0)} \rangle = 0$ and $\langle \Phi_r | \hat{e}_{pq,rs} | \Psi_k^{(0)} \rangle = 0$. Note in passing that some active orbitals of P may disappear in \tilde{P} . Although such situation should in principle be avoided (by reducing P_{\min}), it does not really matter in practice, for their contributions are already contained in the iCISCF(2) energy. For clarity, SDSPT2s is compared with the parent, CAS-based SDSPT2 in Fig. 1.

3.1 Generation of excited CSFs

The n spatial orbitals to be correlated are first partitioned into n_d doubly occupied (DOS), n_a active (AOS), and n_e external (EOS) orbitals. The former two together can be called

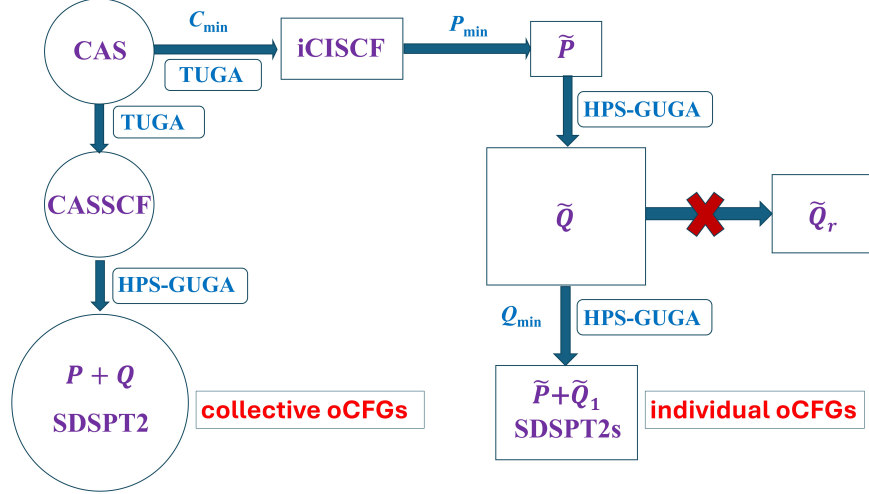


Figure 1: CAS- and selection-based SDSPT2. TUGA: tabulated unitary group approach⁵⁶ for basic coupling coefficients between randomly selected CSFs. $\tilde{Q}_r (= \tilde{Q} - \tilde{Q}_1)$ does not interact with \tilde{P} . Collective/individual oCFGs: collective/individual treatment of reference orbital configurations.

internal orbitals (IOS). In the present context, the orbitals are arranged as $(1, \dots, n_e; n_e + 1, \dots, n_e + n_a; n_e + n_a + 1, \dots, n)$. The reference oCFGs $\{\Phi_R^o\}$ differ only in the occupation numbers $N_{w,R}^o$ of the n_a active orbitals. It is certainly possible to first generate the unique set of singly and doubly excited oCFGs $\{\Phi_q^o\}$, from which the excited CSFs can then be obtained by using, e.g., the genealogical coupling scheme.⁷⁷ However, more efficient is the graphical unitary group approach, where the so-called DRT⁷¹ can be constructed very efficiently for a compressed recording of the excited CSFs. This scheme can further be simplified by observing³² that the partial DRTs for the EOS and DOS can easily be established in advance, for they have at most two electrons and two holes, respectively. As such, one needs to focus only on the sub-DRTs pertinent to the AOS. Specifically, the nodes at level n_e can only be $(0,0) =: V$, $(0,1) =: D$, $(0,2) =: T$, and $(1,0) =: S$ for zero, one, two same-spin, and two opposite-spin electrons in the EOS, respectively. Likewise, the nodes at level $n_e + n_a$ are $(a,b) = (\frac{N_a}{2} - S, 2S) =: \bar{V}$, $(a,b+1) =: \bar{D}$, $(a,b+2) =: \bar{T}$, and $(a+1,b) =: \bar{S}$ for the excitations of zero, one, two same-spin, and two opposite-spin electrons from the DOS to the AOS, respectively. However, these are complete only when the total spin S is zero. When $S = 1/2$, there exists an additional

node $(a + 1, b - 1) =: \bar{D}_{-1/2}$ for the excitation of a beta electron from the DOS to the AOS. In this case, \bar{D} ($= \bar{D}_{1/2}$) refers to the excitation of a single alpha electron from the DOS to the AOS. When $S \geq 1$, still one more node $(a + 2, b - 2) =: \bar{T}_{-1}$ is required for the excitation of two beta electrons from the DOS to the AOS. In this case, there exist 6 nodes, with \bar{T} ($= \bar{T}_{+1}$) representing the excitation of two alpha electrons from the DOS to the AOS. Having determined such nodes for a given spin S , the sub-DRTs ($\bar{X}Y$) ($X, Y = V, D, T, S$) can readily be established by following the **abc-rule** outlined in Sec. S1 in the Supporting Information. It follows that a sub-DRT ($\bar{X}Y$) is composed of nodes and arcs. The nodes are enumerated sequentially from the head \bar{X} (No. $N_{\bar{X}Y}^{\bar{X}}$) to the tail Y (No. $N_{\bar{X}Y}^Y$). A node $(a_w, b_w)_J$ at level w may be connected downward up to four nodes $(a_{w-1}, b_{w-1})_{J_{d\downarrow}}$ at level $w - 1$ via the arcs $J \rightarrow J_{d\downarrow}$ ($d_{\downarrow} \in [0, 3]$). It can also be connected upward to several nodes $(a_{w+1}, b_{w+1})_{J_{d\uparrow}}$ at level $w + 1$ via the possible arcs $J_{d\uparrow} \rightarrow J$ ($d_{\uparrow} \in [0, 3]$). Every node (arc) K can be associated with a weight X_K (Y_{K_d}), so as to identify the in total $\dim(\bar{X}Y)$ possible step vectors $\{(\mathbf{d}_a)_\mu = (d_{n_e+1} \cdots d_{n_e+n_a})_\mu\}$ of the sub-DRT (see Sec. S1 in the Supporting Information). Once this is done, the step vectors $\{\mathbf{d}_\mu = (\mathbf{d}_e \mathbf{d}_a \mathbf{d}_h)_\mu\}$ representing the reference and excited CSFs can readily be established. Here, $(\mathbf{d}_e)_\mu = (d_1 \cdots d_{n_e})_\mu$ and $(\mathbf{d}_h)_\mu = (d_{n_e+n_a+1} \cdots d_{n_e+n_a+n_h})_\mu$ are the partial step vectors for the EOS and DOS, respectively. Note in passing that a bra vector representing $\langle \Phi_\mu |$ is to be written as $\langle \mathbf{d}_\mu | = \langle (\mathbf{d}_h \mathbf{d}_a \mathbf{d}_e)_\mu |$.

As illustrated in Fig. 2 for constructing the CAS(4,3)-based uncontracted MRCISD space of H₂O, the above procedure for constructing the excited CSFs from single and double excitations of a CAS P is truly simple and efficient (see **Algorithm S1** in the Supporting Information). However, the situation is different for a reduced space \tilde{P} to be considered here. The primary reason lies in that one need not pay attention to the reference oCFGs $\{\Phi_R^o\}$ in the case of CAS (for all of them are taken into account automatically), whereas in the case of \tilde{P} , not all reference oCFGs of the CAS are present. A naive procedure is to delete those unwanted CSFs from the CAS-DRT. However, this demands a

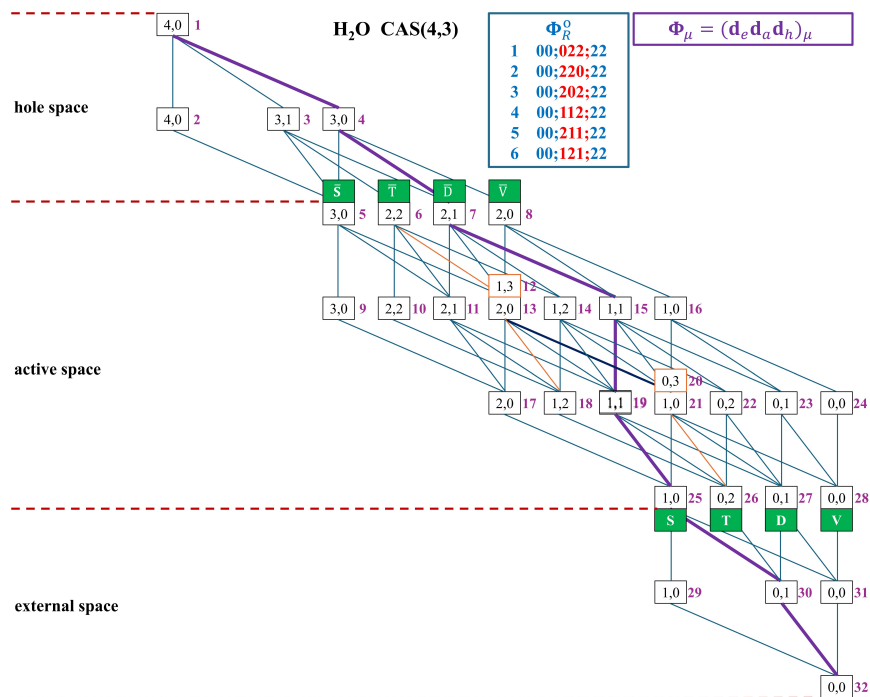


Figure 2: DRT of frozen-core H₂O [$N = 8$, $S = 0$, $n = 7$ (2 hole, 3 active, and 2 external orbitals)]. Inside and outside a box at level r are node (a_r, b_r) and its index J , respectively. The blue solid line connecting two nodes at two adjacent levels is an arc. Nodes at the same site (e.g., 12 and 13; 20 and 21) are distinguished by different colours. The thick black arc indicates that node 12 (13) is connected to node 20 (21). The graphs of the hole and external spaces are symmetric due to hole-particle correspondence. In total 259 reference and excited CSFs are encoded by 32 nodes and their connections. The thick purple arcs from the tail to the head denote the excited CSF $\Phi_{188} = (\mathbf{d}_e \mathbf{d}_a \mathbf{d}_h)_{188} = 1210323$.

CSF-driven algorithm. The merit of GUGA for computing basic coupling coefficients in terms of DRT loops is hence lost completely. It is shown here that the reduced sub-DRTs can be constructed directly by imposing suitable constraints.

To construct a reduced sub-DRT ($\bar{X}Y$), the very first information to be employed is the available number $M_{w,J}$ of electrons associated to each node $(a_w, b_w)_J$, which is just the cumulative number of electrons starting from node Y ($= V, D, T, S$) at level n_e through each level upward to node $(a_w, b_w)_J$, and can simply be calculated as $2a_w + b_w$. It is clear that $M_{n_e, N_{\bar{X}Y}^Y} = 0, 1, 2, 2$ for V, D, T, S and $M_{n_e+n_a, N_{\bar{X}Y}^{\bar{X}}} = N_a, N_a + 1, N_a + 2, N_a + 2, N_a + 1, N_a + 2$ for $\bar{V}, \bar{D}, \bar{T}, \bar{S}, \bar{D}_{-1/2}, \bar{T}_{-1}$, respectively. Going down from level w ($\leq n_e + n_a$) to level $w - 1$ ($\geq n_e + 1$), $M_{w,J}$ can be reduced by $N_{w,J} \in [0, 2]$, leading to $M_{w-1, J_{d\downarrow}}$. Here, $N_{w,J}$ is just the occupation number of several excited oCFGs $\{\Phi_q^o\}$ sharing node $(a_w, b_w)_J$ at level w . However, not all the three values of $N_{w,J}$ are allowed, since the differential occupation $N_{w,J} - N_{w,R}^o$ between the excited $\{\Phi_q^o\}$ and a reference oCFG Φ_R^o cannot be negative. Moreover, when going down from node \bar{X} through each level to node $(a_{w-1}, b_{w-1})_{J_{d\downarrow}}$, the cumulative excitation number $\Delta N_{R, J_{d\downarrow}}^{w-1}$ relative to the reference oCFG Φ_R^o is also limited by the total excitation number $N_{\bar{X}Y}^{ex}$ of sub-DRT ($\bar{X}Y$), as documented in Table 2. $\Delta N_{R, J_{d\downarrow}}^{w-1}$ can be calculated recursively in a top-down manner as

$$\Delta N_{R, J_{d\downarrow}}^{w-1} = \begin{cases} \Delta N_{R, J}^w + (N_{w,J} - N_{w,R}^o) & \text{if } N_{w,J} > N_{w,R}^o, \\ \Delta N_{R, J}^w & \text{if } N_{w,J} \leq N_{w,R}^o, \end{cases} \quad (28)$$

where $w \in [n_e + 2, n_e + n_a]$ and $\Delta N_{R, 1}^{n_e+n_a} = 0$. When $\Delta N_{R, J_{d\downarrow}}^{w-1}$ is greater than the maximum of $N_{\bar{X}Y}^{ex}$, the set of excited oCFGs $\{\Phi_q^o\}$ passing through node $(a_{w-1}, b_{w-1})_{J_{d\downarrow}}$ will be independent of the reference oCFG Φ_R^o . The node $(a_{w-1}, b_{w-1})_{J_{d\downarrow}}$ will be invalid when the minimal value, $\min_R \Delta N_{R, J_{d\downarrow}}^{w-1}$, of the whole set $\mathbf{V}_{w-1} = \{\Delta N_{R, J_{d\downarrow}}^{w-1}; w \in [n_e + 2, n_e + n_a]\}_{R=1}^{N_R^o}$ is greater than $N_{\bar{X}Y}^{ex}$, since in this case all excited oCFGs would have excitation numbers larger than the allowed $N_{\bar{X}Y}^{ex}$. Once the valid $N_{w,J}$ are determined, the allowed step val-

ues $d_w \in [0, 3]$ and hence the arcs $J \rightarrow J_{d\downarrow}$ can be fixed following the **abc-rule** in the Supporting Information.

However, the above procedure still ends up with many redundant intermediate nodes. To see this, we first define the remaining number $M_{w-1,R}^{re}$ of active electrons of the reference oCFG Φ_R^o at level $w - 1$ as

$$M_{w-1,R}^{re} = N_a - \sum_{u=w}^{n_e+n_a} N_{u,R}^o. \quad (29)$$

It is obvious that $M_{w-1,J_{d\downarrow}}$ is bounded by $M_{w-1,R}^{re} + M_{\bar{X}Y}^{ex}$ with $M_{\bar{X}Y}^{ex} = 2$. That $M_{w-1,J_{d\downarrow}} > M_{w-1,R}^{re} + M_{\bar{X}Y}^{ex}$ means that more than two electrons have been excited from the internal orbitals $p \in [w, n]$ of Φ_R^o , thereby rendering Φ_R^o deadwood for the intermediate node $(a_{w-1}, b_{w-1})_{J_{d\downarrow}}$. The survival $\Delta N_{R,J_{d\downarrow}}^{w-1}$ can be collected into the effective set $\mathbf{V}_{w-1}^{eff} = \{\Delta N_{R,J_{d\downarrow}}^{w-1}; w \in [n_e + 2, n_e + n_a]\}$. If the following condition

$$\mathbf{V}_{w-1}^{eff} = \emptyset \text{ or } \min(\mathbf{V}_{w-1}^{eff}) > N_{\bar{X}Y}^{ex} \quad (30)$$

is satisfied, $\{\Phi_q^o\}$ with $N_{w,J}$ will not be generated from single and double excitations from $\{\Phi_R^o\}_{R=1}^{N_R^o}$. The intermediate nodes $(a_{w-1}, b_{w-1})_{J_{d\downarrow}}$ and hence the corresponding arcs $J \rightarrow J_{d\downarrow}$ should be deleted. Moreover, if $w = n_e + 2$, $(a_{w-1}, b_{w-1})_{J_{d\downarrow}}$ must be one of the nodes $(a_{n_e+1}, b_{n_e+1})_d$ ($d \in [0, 3]$) that match Y (see Table 3); otherwise, delete $(a_{w-1}, b_{w-1})_{J_{d\downarrow}}$.

It should also be noted that, while the nodes at different levels are inherently distinct, the nodes at the same level must be made unique by double checking with the existing ones. To achieve this, the multidimensional array $(a_{w-1}, b_{w-1}, \mathbf{V}_{w-1}^{eff})_{J_{d\downarrow}}$ has to be stored. A node $J_{d\downarrow}$ is considered new only if its metadata $(a_{w-1}, b_{w-1}, \mathbf{V}_{w-1}^{eff})$ differs from all the existing ones at the same level $w - 1$. This double checking process is the rate determining step for constructing the reduced sub-DRTs ($\bar{X}Y$). After this, all intermediate nodes of ($\bar{X}Y$) have been generated and \mathbf{V}_{w-1}^{eff} is no longer needed. Starting from Y to \bar{X} , the weights of the nodes can readily be calculated according Eq. (S1). The nodes with the

same weight and downward connecting nodes $J_{d\downarrow}$ are actually identical and should hence be merged together. The survival nodes and corresponding arcs finally form $(\tilde{X}Y)$. As an illustration, the detailed derivations of the reduced sub-DRT ($\tilde{D}S$) for H_2O with one and two oCFGs are documented in Tables 4 and 5, respectively. The results are further plotted in Fig. 3.

The above procedure for constructing the reduced sub-DRTs can be implemented by **Algorithm 1**. Compared with **Algorithm S1** in the Supporting Information for constructing the full sub-DRTs, only lines 11–12 and 14–18 are new, which perform validation of nodes $(a_{w-1}, b_{w-1})_{J_{d\downarrow}}$ [cf. Eqs. (28) and (30)] and double checking, respectively. Since the number of nodes is much less than that of CSFs, the present ‘reduced sub-DRT’ scheme should be more efficient than those working directly with randomly selected CSFs.

Noticeably, $(\tilde{D}V)$ and $(\tilde{V}D)$ are the largest sub-DRTs due to the involvement of three active orbitals (see Table 2). They can be reduced by setting $M_{\tilde{D}V}^{ex} = M_{\tilde{V}D}^{ex} = 1$ in lieu of $M_{\tilde{D}V}^{ex} = M_{\tilde{V}D}^{ex} = 2$. This amounts to screening out some three-active-orbital double (TAOD) excitations that describe the interactions between a hole (in the case of $(\tilde{D}V)$) or particle (in the case of $(\tilde{V}D)$) with an active electron, mediated by the scattering of the other active electrons. It will be shown in Sec. 4.1 that this is a very good approximation (denoted as DVD). However, it is dependent on the ordering of the active orbitals and may hence be used safely only for calculations of vertical excitations.

Algorithm 1. Construction of reduced sub-DRTs

```

01: for  $\bar{X} \in$  nodes at level  $n_e + n_a$  do
02:   for  $Y \in$  nodes at level  $n_e$  do
03:     for  $w \in [n_e + n_a, n_e + 2]$ ;  $w - -$ ; do
04:       search for node  $J_{d\downarrow}$  at level  $w - 1$  from node  $J$  at level  $w$  following the abc-rule
05:       if  $w = n_e + 2$  then
06:         if  $(a_{n_e+1}, b_{n_e+1})$  of  $J_{d\downarrow} = (a_{n_e+1}, b_{n_e+1})_d$  ( $d \in [0, 3]$ ) for  $Y$  in Table 3 then
07:           connect  $J_{d\downarrow}$  with  $Y$ 
08:         else
09:           remove  $J_{d\downarrow}$ 
10:         else
11:           if Eq. (30) is satisfied for the set  $\mathbf{V}_w^{eff}$  then
12:             remove  $J_{d\downarrow}$ 
13:           else
14:             for  $J' < J_{d\downarrow}$  at level  $w - 1$ ;  $J' + +$ ; do
15:               if  $(a_{w-1}, b_{w-1}, \mathbf{V}_{w-1}^e)$  of  $J$  is not equal to  $(a_{w-1}, b_{w-1}, \mathbf{V}_{w-1}^{eff})$  of  $J'$  then
16:                  $J_{d\downarrow}$  is new and connect  $J$  with  $J_{d\downarrow}$ 
17:               else
18:                 remove  $J_{d\downarrow}$  and connect  $J$  with  $J'$ 
19-34: same as Lines 14–29 of Algorithm S1 in the Supporting Information for removing redundant nodes.
35:     for  $w \in [n_e + n_a, n_e + 1]$ ;  $w - -$ ; do
36:       for  $J$  on  $w$ -th level;  $J + +$ ; do
37:         calculate  $X_J$  and  $Y_{J_d}$  of the survival  $J$  and determine the indices of  $(\mathbf{d}_a)_\mu$ 

```

Table 3: Possible upper nodes $(a_{n_e+1}, b_{n_e+1})_d$ of node Y at level n_e

Y	$(a_{n_e+1}, b_{n_e+1})_3$	$(a_{n_e+1}, b_{n_e+1})_2$	$(a_{n_e+1}, b_{n_e+1})_1$	$(a_{n_e+1}, b_{n_e+1})_0$
V	(1,0)		(0,1)	(0,0)
D	(1,1)	(1,0)	(0,2)	(0,1)
T	(1,2)	(1,1)	(0,3)	(0,2)
S	(2,0)		(1,1)	(1,0)

Table 4: Derivation of sub-DRT ($\bar{D}S$) for the orbital configuration $\Phi_1^o = 00;022;22$ of frozen-core H_2O [$N = 8, S = 0, n = 7$ (2 hole, 3 active, and 2 external orbitals)]

J	w	$N_{w,J}$	$N_{w,1}^o$	$\Delta N_{1,J_{d\downarrow}}^{w-1}$	$M_{w-1,J_{d\downarrow}}$	$M_{w-1,1}^{re}$	$J_{d\downarrow}$	(a_{w-1}, b_{w-1})	Inode ^a	Fnode ^b
4	5	0	2	0	5	2	5	(2,1)	no ^c	no
4	5	1	2	0	4	2	6	(2,0)	yes	yes
4	5	1	2	0	4	2	7	(1,2)	yes	no ^e
4	5	2	2	0	3	2	8	(1,1)	yes	yes
6	4	0	2	0	4	0	9	(2,0)	no ^c	no
6	4	1	2	0	3	0	10	(1,1)	no ^c	no
6	4	2	2	0	2	0	11	(1,0)	yes	yes
7	4	0	2	0	4	0	12	(1,2)	no ^d	no
7	4	1	2	0	3	0	13	(1,1)	no ^c	no
7	4	1	2	0	3	0	14	(0,3)	no ^d	no
7	4	2	2	0	2	0	15	(0,2)	no ^d	no
8	4	0	2	0	3	0	16	(1,1)	no ^c	no
8	4	1	2	0	2	0	17	(1,0)	yes	no ^e
8	4	1	2	0	2	0	18	(0,2)	no ^d	no
8	4	2	2	0	1	0	19	(0,1)	no ^d	no
11	3	0	0	0	2	0	20	(1,0)	yes	yes
17	3	0	0	0	2	0	21	(1,0)	yes	no ^f

^a Intermediate node; ^b Final node; ^c $\mathbf{V}_{w-1}^{eff} = \emptyset$ in Eq. (30); ^d (a_{n_e+1}, b_{n_e+1}) of $J_{d\downarrow} \neq (a_{n_e+1}, b_{n_e+1})_d$ ($d \in [0, 3]$) for $Y = S$ in Table 3; ^e disconnected; ^f merged.

Table 5: Derivation of sub-DRT ($\bar{D}S$) for the orbital configurations $\Phi_1^o = 00;022;22$ and $\Phi_2^o = 00;220;22$ of frozen-core H₂O [$N = 8, S = 0, n = 7$ (2 hole, 3 active, and 2 external orbitals)]

J	w	$N_{w,J}$	$N_{w,1}^o$	$N_{w,2}^o$	$\Delta N_{1,J_{d\downarrow}}^{w-1}$	$\Delta N_{2,J_{d\downarrow}}^{w-1}$	$M_{w-1,J_{d\downarrow}}$	$M_{w-1,1}^{re}$	$M_{w-1,2}^{re}$	$J_{d\downarrow}$	(a_{w-1}, b_{w-1})	Inode ^a	Fnode ^b
4	5	0	2	0	0	0	5	2	4	5	(2,1)	yes	yes
4	5	1	2	0	0	1	4	2	4	6	(2,0)	yes	yes
4	5	1	2	0	0	1	4	2	4	7	(1,2)	yes	no ^e
4	5	2	2	0	0	2	3	2	4	8	(1,1)	yes	yes
5	4	0	2	2	0	0	5	0	2	9	(2,1)	no ^c	no
5	4	1	2	2	0	0	4	0	2	10	(2,0)	yes	yes
5	4	1	2	2	0	0	4	0	2	11	(1,2)	no ^c	no
5	4	2	2	2	0	0	3	0	2	12	(1,1)	yes	yes
6	4	0	2	2	0	1	4	0	2	13	(2,0)	yes	no ^e
6	4	1	2	2	0	1	3	0	2	14	(1,1)	yes	no ^e
6	4	2	2	2	0	1	2	0	2	15	(1,0)	yes	yes
7	4	0	2	2	0	1	4	0	2	16	(1,2)	no ^c	no
7	4	1	2	2	0	1	3	0	2	17	(1,1)	yes	no ^e
7	4	1	2	2	0	1	3	0	2	18	(0,3)	no ^c	no
7	4	2	2	2	0	1	2	0	2	19	(0,2)	no ^c	no
8	4	0	2	2	0	2	3	0	2	20	(1,1)	yes	no ^e
8	4	1	2	2	0	2	2	0	2	21	(1,0)	yes	no ^f
8	4	1	2	2	0	2	2	0	2	22	(0,2)	no ^c	no
8	4	2	2	2	0	2	1	0	2	23	(0,1)	no ^c	no
10	3	2	0	2	2	0	2	0	0	24	(1,0)	yes	yes
12	3	1	0	2	1	0	2	0	0	25	(1,0)	yes	no ^f
13	3	2	0	2	2	1	2	0	0	26	(1,0)	no ^d	no
14	3	1	0	2	1	1	2	0	0	27	(1,0)	no ^d	no
15	3	0	0	2	0	1	2	0	0	28	(1,0)	yes	no ^f
17	3	1	0	2	1	1	2	0	0	29	(1,0)	no ^d	no
20	3	1	0	2	1	2	2	0	0	30	(1,0)	no ^d	no
21	3	0	0	2	0	2	2	0	0	31	(1,0)	yes	no ^f

^a Intermediate node; ^b Final node; ^c (a_{n_e+1}, b_{n_e+1}) of $J_{d\downarrow} \neq (a_{n_e+1}, b_{n_e+1})_d$ ($d \in [0, 3]$) for $Y = S$ in Table 3; ^d $\min_R(\mathbf{V}_{w-1}^{eff}) > N_{DS}^{ex} = 0$ in Eq. (30); ^e disconnected; ^f merged.

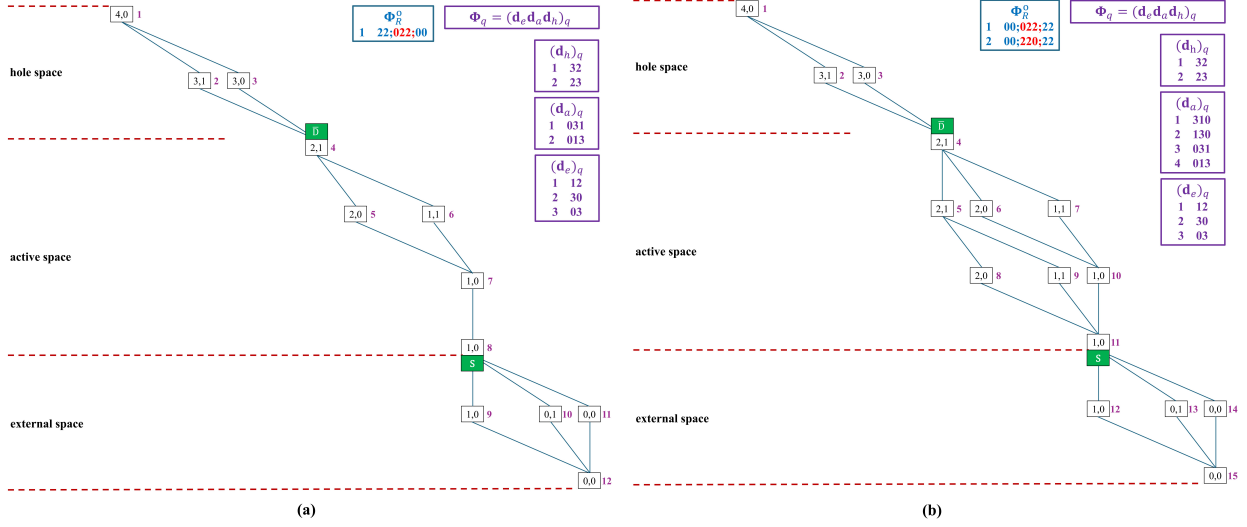


Figure 3: Reduced sub-DRT ($\bar{D}S$) of frozen-core H₂O [$N = 8$, $S = 0$, $n = 7$ (2 hole, 3 active, and 2 external orbitals)]. (a) one reference oCFG (Φ_R^0); (b) two reference oCFGs. Inside and outside a box at level r are node (a_r, b_r) and its index J , respectively. The blue solid line connecting two nodes at two adjacent levels is an arc. $\{\Phi_q\}$ are excited CSFs.

3.2 Matrix elements

What has been discussed so far is how to generate the excited CSFs. However, even for the reduced reference space \tilde{P} , the use of individual CSFs as perturbors is still prohibitively expensive. In contrast, the use of internally contracted configurations (ICC) is more effective,⁶⁸ for they are known to span exactly the FOIS, even though the number of them is only related to the number of active orbitals but independent of the number of reference CSFs. In the parlance of HPS-GUGA, the ICCs are defined as³³

$$\begin{aligned} \bar{\Phi}_{Mk}^{\bar{X}Y} &= \hat{E}_M |\Psi_k^{(0)}\rangle, \quad \hat{E}_M = \hat{E}_{pq}, \hat{e}_{pq,rs} \in \bar{X}Y \\ &= \sum_{q \in \bar{X}Y} |\Phi_q\rangle C_{qM}^k, \end{aligned} \quad (31)$$

$$C_{qM}^k = \langle \Phi_q | \hat{E}_M | \Psi_k^{(0)} \rangle = \sum_{R \in \bar{V}V} \langle \Phi_q | \hat{E}_M | \Phi_R \rangle \bar{C}_{Rk}^{(0)}, \quad (32)$$

where the excitation operators have been defined in Table 2. The internal contraction coefficients C_{qM}^k ($q \in \bar{X}Y$) can be reexpressed as³³

$$C_{qM}^k = \sum_{R \in \bar{V}V} \langle (\mathbf{d}_h \mathbf{d}_a \mathbf{d}_e)_q | \hat{E}_M | (\mathbf{d}_e \mathbf{d}_a \mathbf{d}_h)_R \rangle \bar{C}_{Rk}^{(0)} \quad (33)$$

$$= ELS(YV) \cdot HLS(\bar{X}\bar{V}) \cdot A_{q_a M}^k, \quad (34)$$

$$A_{q_a M}^k = \sum_{R_a \in (\bar{V}V)} ALS(\bar{X}Y, \bar{V}V)_{q_a R_a} \bar{C}_{R_a k}^{(0)}. \quad (35)$$

Here, q_a and R_a are the lexical orders of step vectors $(\mathbf{d}_a)_q$ and $(\mathbf{d}_a)_{R_a}$, respectively (see Sec. S1 in the Supporting Information). $ELS(YV)$ (involving only external orbitals) and $HLS(\bar{X}\bar{V})$ (involving only doubly occupied orbitals) are the external and hole loop shapes, respectively, and can be pre-computed.³³ As a result, the searching for loops needs to be performed only within the AOS, which involves much fewer partial loops compared to the implementation without using the hole-particle correspondence. Note that multiple $ALS(\bar{X}Y, \bar{V}V)_{q_a R_a}$ with identical active orbitals can be searched simultaneously on the fly and contracted with $\bar{C}_{Rk}^{(0)}$ in parallel with respect to partial loops (which are defined by the ranges of the indices of the excitation operators, see Table 2 and Figures 2 and 3 in Ref. 56).

The ICCs $\{\bar{\Phi}_{Mk}^{\bar{X}Y}\}$ are not orthogonal to each other and are even linearly dependent. Therefore, a canonical orthonormalization has to be carried out. Since both $HLS(\bar{X}\bar{V})$ and $ELS(YV)$ are just factors, they can be absorbed in the orthonormalization procedure. As such, the contraction coefficients C_{qM}^k can simply be set to $A_{q_a M}^k$ (35), which can be stored as a sparse matrix for each state k . Those excited CSFs Φ_q with zero coefficients C_{qM}^k belong to the non-interacting external space \tilde{Q}_r and will hence be discarded.

As stated before, the $(\bar{D}V)$ and $(\bar{V}D)$ subspaces are memory intensive, due to the fact that the numbers of coefficients $A_{q_a M}^k$ (35) scale as $n_a^3 \times \dim(\bar{V}D)$ and $n_a^3 \times \dim(\bar{D}V)$, respectively. Apart from the previous DVD approximation, an integral-driven elimination

of unimportant TAODs can further be introduced, viz.,

$$\max_{p,R \in \bar{V}V} (|(pu|vw) \cdot \langle (\mathbf{d}_h \mathbf{d}_a \mathbf{d}_e)_q | \hat{e}_{pu,vw} | \Phi_R \rangle \bar{C}_{Rk}^{(0)}|) < Q_{\min}, \quad (36)$$

where p refers to a doubly occupied and an external orbital for sub-DRTs ($\bar{D}V$) and ($\bar{V}D$), respectively, and Q_{\min} is the prechosen threshold. Note that Eq. (36) eliminates TAODs in batches instead of individually. That is, given a partial step vector \mathbf{d}_a [i.e., a specific triple (u, vw) in the expression (36)] and a partial step vector $\mathbf{d}_e / \mathbf{d}_h$, all TAODs $(\mathbf{d}_h \mathbf{d}_a \mathbf{d}_e)_q$ with different $(\mathbf{d}_h)_q / (\mathbf{d}_e)_q$ are pruned away if the condition (36) holds in the case of ($\bar{D}V$)/($\bar{V}D$). It will be shown in Sec. 4.1 that such prescreening reduces the number of TAODs substantially and hence also the number of ICCs. However, experimentations reveal that similar prescreenings cannot be applied to the other CI subspaces.

The coupling coefficients between the ICCs can be calculated as

$$\begin{aligned} \langle \bar{\Phi}_{Mk}^{\bar{X}Y} | \hat{E}_M | \bar{\Phi}_{Nk}^{\bar{X}'Y'} \rangle &= \sum_{\mu \in \bar{X}Y, \nu \in \bar{X}'Y'} C_{\mu M}^k \langle \Phi_\mu | \hat{E}_M | \Phi_\nu \rangle C_{\nu N}^k \\ &= EL S(Y Y') \cdot HLS(\bar{X} \bar{X}') \cdot \mathbf{ALSC}_{MN}^k, \end{aligned} \quad (37)$$

$$\begin{aligned} \mathbf{ALSC}_{MN}^k &= \sum_{\mu_a \in \bar{X}Y, \nu_a \in \bar{X}'Y'} A_{\mu_a M}^k \cdot ALS(\bar{X}Y, \bar{X}'Y')_{\mu_a \nu_a} \cdot A_{\nu_a N}^k \\ &= [(\mathbf{A}^k)^\dagger \cdot \mathbf{ALS} \cdot \mathbf{A}^k]_{MN}, \end{aligned} \quad (38)$$

where \mathbf{ALSC}^k represents the assembled matrix of internally contracted partial loops for each state k .

4 Results and Discussion

The spin-free exact two-component (sf-X2C) relativistic Hamiltonian^{78,79} was employed throughout to account for scalar relativistic effects. The iCISCF(2)⁶⁶ calculations, which took a single parameter (C_{\min}) to prune away unimportant CSFs during the iterations,

were initiated and governed by the iCAS (imposed selection of CAS) approach.⁸⁰ Upon convergence, the contributions of the discarded CSFs (within the CAS) to the energy were accounted for via ENPT2, leading to $E_k^{(0)}$. Those CSFs in the iCISCF wavefunctions $\Psi_k^{(0)}$ were further discarded if their coefficients are smaller in absolute value than P_{\min} for all the target states. The Dyll Hamiltonian was then diagonalized in the resulting \tilde{P} space, leading to $\tilde{\Psi}_k^{(0)}$ and $\tilde{E}_k^{(0)}$ for subsequent SDSPT2s calculations of dynamic correlation energies $E_k^{(2)}$, where the TAODs were screened as discussed before. The SDSPT2s total energies reported here refer to $E_k^{(0)} + E_k^{(2)}$, which is to be compared with $\tilde{E}_k^{(0)} + E_k^{(2)}$ as advocated in Ref 81. The corresponding NEVPT2s results were obtained automatically. All calculations were performed with the BDF program package^{82–85} on a computer equipped with 2 Intel(R) Xeon(R) Platinum 8375C CPUs (64 cores in total) and 1 TB memory.

4.1 Cutoff Thresholds C_{\min} , P_{\min} , Q_{\min} , and DVD

A simplified model of heme (denoted as $\text{Fe}^{\text{II}}\text{L}_2$ with L being $\text{N}_2\text{C}_3\text{H}_4$)^{86,87} was first taken as a showcase to reveal the effectiveness of the cutoff thresholds, including C_{\min} , P_{\min} , Q_{\min} , and DVD (see the end of Sec. 3.1). The cartesian coordinates were taken from Ref. 86 (see also Tables S2–S4 in the Supporting Information). The iCISCF(14,17) calculations were performed for the 5A_g , $^3B_{3g}$, and 1A_g states separately. As shown in Fig. S1, the active orbitals include Fe $3d4s4d$ and two σ , two π , and two π^* orbitals composed of N $2p_{x,y}$ in the molecular plane. The $1s$ orbital of C and N as well as the $1s2s2p$ orbitals of Fe were frozen in the SDSPT2s calculations. The def2-TZVP⁸⁸ and corresponding auxiliary basis sets⁸⁹ for the resolution of identity (RI) approximation were employed in both the iCISCF and SDSPT2s calculations.

It is first seen from Table 6 that iCISCF(2) converges steadily to CASSCF as C_{\min} decreases. It can also be seen from Table 7 that the SDSPT2s energies are only weakly dependent on C_{\min} , and a value of 10^{-4} for C_{\min} is already sufficient, which is in line with

the previous findings.⁶⁶ In this case, the number of CSFs in the reference space is merely a few of ten thousands of that of CAS(14,17) as shown in Table 8. It is also of interest to see from Table 7 that the DVD approximation does not affect discernibly the spin gaps, even though ca. 25% of the TAODs have been pruned away (see Table 8). It appears that the smaller the C_{\min} , the less effective the DVD. This is not surprising, for a smaller C_{\min} implies more reference oCFGs and hence more survival intermediate nodes before the DVD condition is met. The results in Table 9 merely show that SDSPT2s is rather insensitive to P_{\min} , and $P_{\min} = 10^{-3}$ is already sufficient. On top of this, a value of 10^{-5} for Q_{\min} can be invoked to further screen the TAODs, as can be seen from Table 10. Note in passing that the use of Q_{\min} eliminates a large number of individual excited CSFs but does not reduce the number of ICCs very much. This explains the robustness of such integral-based screening. Unless otherwise stated, ($C_{\min} = 10^{-4}$, $P_{\min} = 10^{-3}$, DVD, $Q_{\min} = 10^{-5}$) will be taken as the default setting in subsequent calculations. With this setting, SDSPT2s yields 4.1 and 38.7 kcal/mol for the gaps between 5A_g and ${}^3B_{3g}$ and between 5A_g and 1A_g of $\text{Fe}^{\text{II}}\text{L}_2$, respectively, which are in good agreement with those (3.8 and 40.7 kcal/mol) by CCSD.⁸⁶

Table 6: iCISCF(14,17) energies ($+1725.0 E_h$) of $\text{Fe}^{\text{II}}\text{L}_2$ with sf-X2C/def2-TZVP

C_{\min}	$E_{\text{var}}^{(0)}({}^5A_g)^a$	$E^{(0)}({}^5A_g)^b$	$E_{\text{var}}^{(0)}({}^3B_{3g})^a$	$E^{(0)}({}^3B_{3g})^b$	$E_{\text{var}}^{(0)}({}^1A_g)^a$	$E^{(0)}({}^1A_g)^b$
1.0×10^{-3}	-0.489530	-0.494016	-0.465730	-0.473060	-0.418774	-0.425355
5.0×10^{-4}	-0.491718	-0.494107	-0.469025	-0.473359	-0.421739	-0.425385
1.0×10^{-4}	-0.493753	-0.494260	-0.472586	-0.473590	-0.423578	-0.424461
5.0×10^{-5}	-0.493983	-0.494275	-0.473023	-0.473627	-0.423964	-0.424486
0.0	-0.494286	-0.494286	-0.473641	-0.473641	-0.424498	-0.424498

^a $E_{\text{var}}^{(0)}$: variational energy; ^b $E^{(0)}$: $E_{\text{var}}^{(0)}$ plus inner space ENPT2 correction.

Table 7: Dependence of SDSPT2s energies (+1727.0 E_h) of $\text{Fe}^{\text{II}}\text{L}_2$ on C_{min} and DVD [sf-X2C/def2-TZVP, iCISCF(14,17), $P_{\text{min}} = C_{\text{min}}$, $Q_{\text{min}} = 0.0$]

C_{min}	$E(^5A_g)$	$E(^3B_{3g})$	$E(^1A_g)$	ΔE_1^{a}	ΔE_2^{b}
$E = E_k^{(0)} + E_k^{(2)}, \text{w/o DVD}$					
1.0×10^{-3}	-0.505898	-0.498242	-0.437672	4.8	42.8
5.0×10^{-4}	-0.506027	-0.498808	-0.437506	4.5	43.0
1.0×10^{-4}	-0.505800	-0.499096	-0.444090	4.2	38.7
5.0×10^{-5}	-0.505916	-0.499364	-0.444459	4.1	38.6
$E = E_k^{(0)} + E_k^{(2)}, \text{w/ DVD}$					
1.0×10^{-3}	-0.505526	-0.497677	-0.436842	4.9	43.1
5.0×10^{-4}	-0.505852	-0.498517	-0.437150	4.6	43.1
1.0×10^{-4}	-0.505751	-0.499040	-0.444233	4.2	38.6
5.0×10^{-5}	-0.505895	-0.499348	-0.444503	4.1	38.5
$E = \tilde{E}_k^{(0)} + E_k^{(2)}, \text{w/o DVD}$					
1.0×10^{-3}	-0.501337	-0.491265	-0.431151	6.3	44.0
5.0×10^{-4}	-0.503629	-0.494369	-0.434203	5.8	43.6
1.0×10^{-4}	-0.505372	-0.498232	-0.443284	4.5	39.0
5.0×10^{-5}	-0.505660	-0.498849	-0.443993	4.3	38.7
$E = \tilde{E}_k^{(0)} + E_k^{(2)}, \text{w/ DVD}$					
1.0×10^{-3}	-0.500965	-0.490700	-0.430335	6.4	44.3
5.0×10^{-4}	-0.503454	-0.494082	-0.433846	5.9	43.7
1.0×10^{-4}	-0.505291	-0.498184	-0.443422	4.5	38.8
5.0×10^{-5}	-0.505639	-0.498832	-0.444037	4.3	38.7

^a energy gap (in kcal/mol) between 5A_g and $^3B_{3g}$; ^b energy gap (in kcal/mol) between 5A_g and 1A_g .

Table 8: Numbers of parameters (as function of C_{\min} and DVD) in SDSPT2s calculations of $\text{Fe}^{\text{II}}\text{L}_2$ [sf-X2C/def2-TZVP, iCISCF(14,17), $P_{\min} = C_{\min}$, $Q_{\min} = 0.0$]

C_{\min}	$N_R/N_{CAS} \times 10^4$ ^a	N_1 ^b	N_2/N_1 (%) ^c	N_3 ^d	N_4/N_3 (%) ^e
			⁵ A_g		
1.0×10^{-3}	0.2	1473684	69.8	29652784	73.1
5.0×10^{-4}	0.4	4643615	70.9	87211642	75.1
1.0×10^{-4}	1.44	13096536	71.6	251826337	74.7
5.0×10^{-5}	2.33	20281378	73.7	383337864	78.1
			³ B_{3g}		
1.0×10^{-3}	0.2	2555799	69.5	40553046	72.0
5.0×10^{-4}	0.4	8783390	72.6	121732995	73.6
1.0×10^{-4}	1.6	23520762	76.6	328815443	77.4
5.0×10^{-5}	2.9	39305048	77.7	539232278	79.9
			¹ A_g		
1.0×10^{-3}	0.6	2630783	66.4	20620925	65.8
5.0×10^{-4}	1.1	6460877	66.8	48328424	64.5
1.0×10^{-4}	4.5	21965386	74.4	168755703	75.2
5.0×10^{-5}	7.8	38131568	75.5	286693520	77.0

^a N_R : number of selected reference CSFs; N_{CAS} : number of CAS reference CSFs (13009252, 18804520, and 9690780 for ⁵ A_g , ³ B_{3g} , and ¹ A_g , respectively); ^b N_1 : number of $\tilde{Q}_1(\tilde{D}V)$ without DVD; ^c N_2 : number of $\tilde{Q}_1(\tilde{D}V)$ with DVD; ^d N_3 : number of $\tilde{Q}_1(\tilde{V}D)$ without DVD; ^e N_4 : number of $\tilde{Q}_1(\tilde{V}D)$ with DVD.

Table 9: Dependence of SDSPT2s energies ($+1727.0 E_h$) of $\text{Fe}^{\text{II}}\text{L}_2$ on P_{\min} [sf-X2C/def2-TZVP, iCISCF(14,17), $C_{\min} = 10^{-4}$, $Q_{\min} = 0.0$, DVD]

P_{\min}	$E(^5A_g)$	$E(^3B_{3g})$	$E(^1A_g)$	ΔE_1^a	ΔE_2^b
			$E = E_k^{(0)} + E_k^{(2)}$		
1.0×10^{-3}	-0.506706	-0.500335	-0.445045	4.0	38.7
5.0×10^{-4}	-0.505963	-0.499160	-0.444192	4.3	38.8
1.0×10^{-4}	-0.505751	-0.499040	-0.444233	4.2	38.6
			$E = \tilde{E}_k^{(0)} + E_k^{(2)}$		
1.0×10^{-3}	-0.503998	-0.495798	-0.440368	5.1	39.9
5.0×10^{-4}	-0.504875	-0.497441	-0.442269	4.7	39.3
1.0×10^{-4}	-0.505290	-0.498184	-0.443423	4.5	38.8

^a energy gap (in kcal/mol) between ⁵ A_g and ³ B_{3g} ; ^b energy gap (in kcal/mol) between ⁵ A_g and ¹ A_g .

Table 10: Numbers of parameters and energies (as function of Q_{\min}) in SDSPT2s calculations of $\text{Fe}^{\text{II}}\text{L}_2$ [sf-X2C/def2-TZVP, iCISCF(14,17), $C_{\min} = 10^{-4}$, $P_{\min} = 10^{-3}$, DVD]

	Q_{\min}			
	1.0×10^{-3}	1.0×10^{-4}	1.0×10^{-5}	0.0
$N_{\bar{\text{D}}\text{V}}/\bar{N}_{(\bar{\text{D}}\text{V})}$ of ${}^5A_g^{\text{a}}$	162569/4049	348874/12443	1139368/17236	3835035/18391
$N_{\bar{\text{V}}\text{D}}/\bar{N}_{(\bar{\text{V}}\text{D})}$ of ${}^5A_g^{\text{b}}$	3348671/35627	3964792/105844	10823677/199235	78491786/236659
$N_{\bar{\text{D}}\text{V}}/\bar{N}_{(\bar{\text{D}}\text{V})}$ of ${}^3B_{3g}^{\text{a}}$	162183/4829	473459/13820	2081959/17716	6143488/18427
$N_{\bar{\text{V}}\text{D}}/\bar{N}_{(\bar{\text{V}}\text{D})}$ of ${}^3B_{3g}^{\text{b}}$	3895457/35512	4788344/114775	13692840/202556	92404719/237653
$N_{\bar{\text{D}}\text{V}}/\bar{N}_{(\bar{\text{D}}\text{V})}$ of ${}^1A_g^{\text{a}}$	220640/5644	560727/14516	2215580/17826	4770647/18384
$N_{\bar{\text{V}}\text{D}}/\bar{N}_{(\bar{\text{V}}\text{D})}$ of ${}^1A_g^{\text{b}}$	1548920/36238	2330557/117176	8106330/202719	34877101/234687
	$E = E_k^{(0)} + E_k^{(2)}$			
$E({}^5A_g)^{\text{c}}$	-0.502386	-0.505569	-0.506566	-0.506706
$E({}^3B_{3g})^{\text{c}}$	-0.492765	-0.498354	-0.500099	-0.500335
$E({}^1A_g)^{\text{c}}$	-0.438914	-0.443763	-0.444933	-0.445045
ΔE_1^{d}	6.0	4.5	4.1	4.0
ΔE_2^{e}	39.8	38.8	38.7	38.7
	$E = \tilde{E}_k^{(0)} + E_k^{(2)}$			
$E({}^5A_g)^{\text{c}}$	-0.499678	-0.502862	-0.503859	-0.503998
$E({}^3B_{3g})^{\text{c}}$	-0.488228	-0.493817	-0.495562	-0.495798
$E({}^1A_g)^{\text{c}}$	-0.434237	-0.439087	-0.440256	-0.440368
ΔE_1^{d}	7.2	5.7	5.2	5.1
ΔE_2^{e}	41.1	40.0	39.9	39.9

^a $N_{\bar{\text{D}}\text{V}}$: number of $\tilde{Q}_1(\bar{\text{D}}\text{V})$; $\bar{N}_{(\bar{\text{D}}\text{V})}$: number of $\Phi_{Mk}^{\bar{\text{D}}\text{V}}$ (see Eq. (31)); ^b $N_{\bar{\text{V}}\text{D}}$: number of $\tilde{Q}_1(\bar{\text{V}}\text{D})$; $\bar{N}_{(\bar{\text{V}}\text{D})}$: number of $\Phi_{Mk}^{\bar{\text{V}}\text{D}}$ (see Eq. (31)); ^c total energy shifted by 1727.0 E_h ; ^d energy gap (in kcal/mol) between 5A_g and ${}^3B_{3g}$; ^e energy gap (in kcal/mol) between 5A_g and 1A_g .

4.2 Computational Resources

To see the gain in efficiency of SDSPT2s over SDSPT2, we carried out calculations for the ground and lowest triplet states of anthracene with the cc-pVDZ basis set⁹⁰ and D_{2h} symmetry. The geometry of anthracene was taken from Ref. 91. The (14e, 14o) active space is composed of the valence π and π^* orbitals. As can be seen from Table 11, except for the construction of the sub-DRTs, all other steps became significantly cheaper by incorporating the cutoffs, leading to an overall gain in efficiency by more than one order of

magnitude, yet without sacrificing the accuracy. In particular, the memory requirement is also reduced substantially.

Table 11: Detailed information for CAS(14,14)-SDSPT2/cc-pVDZ calculations of the S_0 and T_1 states of anthracene

	S_0^a	S_0^b	T_1^a	T_1^b
T_{DRT}/s^c	147	15	231	19
$T_{\Psi_k^{(0)}}/s^d$	3	615	14	2693
$T_{\Phi_{Mk}^{\bar{X}Y}}/s^e$	178	1129	632	3422
$T_{\Psi_{q,k}^{(0)}}/s^f$	1390	17471	4063	36481
$T_{\Xi_k^{(1)}}/s^g$	123	4482	430	10646
$T_{\Theta_k^{(2)}}/s^h$	124	5609	438	14051
$T_{\tilde{S}}/s^i$	24	321	58	636
$T_{\tilde{H}}/s^j$	244	9030	863	21339
T_{tot}/s^k	2234	38671	6729	89287
M_{max}/GB^l	0.5	5.8	0.9	11.4
N_R^m	6725	691160	17158	1252895
N_q^n	4.751×10^{10}	6.134×10^{12}	2.143×10^{11}	1.327×10^{13}
E^o	-0.834178 (-0.829521)	-0.829089	-0.763068 (-0.756254)	-0.755786
ΔE^p	0.0 (0.0)	0.0	44.6 (46.0)	46.0

^a SDSPT2s ($C_{\min} = 10^{-4}$, $P_{\min} = 10^{-3}$, $Q_{\min} = 10^{-5}$, DVD); ^b SDSPT2; ^c time for constructing (reduced) sub-DRTs (see **Algorithm 1** or **Algorithm S1**); ^d time for calculating $\Psi_k^{(0)}$; ^e time for calculating ICC $\Phi_{Mk}^{\bar{X}Y}$ [see Eq. (31); including generation of \tilde{Q}_1 [see Eq. (36)] in the case of SDSPT2s]; ^f time for calculating $\Psi_{q,k}^{(0)}$ [see Eq.(11)]; ^g time for calculating $\Xi_k^{(1)}$ [see Eq. (4)]; ^h time for calculating $\Theta_k^{(2)}$ [see Eq. (6)]; ⁱ time for constructing \tilde{S} [see Eq. (15)]; ^j time for constructing \tilde{H} [see Eq. (14)]; ^k total time; ^l peak memory; ^m dimension of \tilde{P} or P ; ⁿ dimension of \tilde{Q}_1 or Q ; ^o total energy shifted by 537.0 E_h ; in parentheses are $\tilde{E}_k^{(0)} + E_k^{(2)}$; ^p relative energy (in kcal/mol) with respect to S_0 ; in parentheses are derived from $\tilde{E}_k^{(0)} + E_k^{(2)}$.

4.3 Size Consistency

It has been shown⁵⁹ that the size-consistency errors of SDSPT2 can be largely removed by using the Pople correction.⁷³ To see if this is also the case for SDSPT2s, we calculated the three lowest singlet and three lowest triplet states of the anthracene...Rg complexes, with Rg (= He, Ne, Ar, Kr) set to 100 Å away from the center of anthracene. Three-state-averaged (SA3) CAS/iCISCF(14,14) calculations were first performed with the cc-pVDZ basis set⁹⁰ and C_{2v} symmetry. It can be seen from Table 12 that the size-consistency er-

rors of SDSPT2s are indeed very much the same as those of CAS-based SDSPT2. Note in passing that, at variance with the state-specific NEVPT2 (which is strictly size consistent⁵), MS-NEVPT2s/NEVPT2 is also not size consistent but the errors are much smaller than those of SDSPT2s/SDSPT2. Yet, the advantage of SDSPT2s/SDSPT2 lies in the unified treatment of single and multiple states, which is particularly warranted for situations

with near degeneracies.⁵⁵

Table 12: Size-consistency errors (in meV) of SA3-iCISCF(14,14), MS-NEVPT2s, and SDSPT2s for the excitation energies (relative to anthracene) of the low-lying singlet and triplet states of anthracene...Rg (Rg = He, Ne, Ar, Kr set to 100 Å away from the center of anthracene; cc-pVDZ; $C_{\min} = 10^{-4}$, $P_{\min} = 10^{-3}$, $Q_{\min} = 10^{-5}$, DVD)

Species	iCISCF	MS-NEVPT2s ^a	MS-NEVPT2	SDSPT2s ^{a,b}	SDSPT2 ^b
Singlet					
anthracene... He $1^1 A_1$	0.0	0.1 (0.0)	0.0	1.9 (2.6)	1.8
anthracene... He $2^1 A_1$	0.0	2.5 (2.2)	2.6	4.0 (3.4)	4.0
anthracene... He $3^1 A_1$	0.0	2.4 (2.1)	1.9	4.4 (7.1)	3.8
anthracene... Ne $1^1 A_1$	0.0	0.3 (0.0)	0.0	-2.0 (-39.3)	-2.3
anthracene... Ne $2^1 A_1$	0.0	1.9 (1.7)	2.6	-1.7 (-2.3)	-1.5
anthracene... Ne $3^1 A_1$	0.0	2.7 (2.3)	1.9	1.8 (2.8)	1.0
anthracene... Ar $1^1 A_1$	0.0	0.2 (0.0)	0.0	30.2 (28.3)	29.7
anthracene... Ar $2^1 A_1$	0.0	2.4 (2.2)	2.7	31.4 (31.1)	30.7
anthracene... Ar $3^1 A_1$	0.0	2.3 (1.9)	2.7	33.8 (33.4)	33.5
anthracene... Kr $1^1 A_1$	0.0	0.3 (0.1)	0.0	95.6 (68.8)	94.6
anthracene... Kr $2^1 A_1$	0.0	2.9 (2.3)	2.5	97.2 (98.0)	94.9
anthracene... Kr $3^1 A_1$	0.0	2.7 (2.0)	1.7	100.3 (99.4)	97.2
Triplet					
anthracene... He $1^3 A_1$	0.2	-5.3 (0.0)	1.3	-3.1 (2.2)	3.0
anthracene... He $2^3 A_1$	0.1	0.0 (0.3)	2.1	1.7 (2.6)	3.8
anthracene... He $3^3 A_1$	0.0	6.2 (2.4)	2.0	7.7 (2.7)	3.6
anthracene... Ne $1^3 A_1$	0.0	1.3 (1.7)	1.3	-1.1 (-1.3)	-1.4
anthracene... Ne $2^3 A_1$	0.0	6.2 (3.0)	2.1	3.8 (0.8)	-0.3
anthracene... Ne $3^3 A_1$	0.0	8.0 (4.1)	2.1	5.5 (0.5)	-0.4
anthracene... Ar $1^3 A_1$	0.2	-6.4 (0.1)	1.2	24.3 (30.7)	30.6
anthracene... Ar $2^3 A_1$	0.1	-0.1 (0.5)	2.1	30.3 (30.7)	31.7
anthracene... Ar $3^3 A_1$	0.0	8.8 (3.8)	2.1	38.0 (32.9)	30.8
anthracene... Kr $1^3 A_1$	0.3	-12.6 (-1.7)	1.3	84.4 (94.9)	95.5
anthracene... Kr $2^3 A_1$	0.1	-5.6 (-1.4)	2.1	90.7 (94.9)	96.4
anthracene... Kr $3^3 A_1$	0.0	7.6 (2.4)	2.2	101.5 (95.4)	94.5

^a Results in parentheses were derived from $E_k^{(0)} + E_k^{(2)}$

^b With Pople correction.

4.4 PEC of Cr₂

The potential energy curve (PEC) of Cr₂ has been investigated extensively in the last decades.⁹²⁻¹⁰⁰ The CAS(12,12) PEC turns out to be repulsive, which is qualitatively wrong. Therefore, it is mandatory to use larger active spaces, e.g., CAS(12,22)⁹⁶ (*3d4s4d*), CAS(12,28)⁹⁷ (*3d4s4d4p*), and even CAS(12,42)⁹⁸ (*3d4s4d4p4f*) in multi-reference calculations. Here, we used the CAS(12,22) active space, in conjunction with the cc-pwCV5Z-DK basis set¹⁰¹ and *D*_{2h} symmetry. The SDSPT2s and NEVPT2s PECs are plotted in Fig. 4, along with those by DMRG(12,22)-SC-NEVPT2 (DMRG: density matrix renormalization group; SC: strong contraction),⁹⁶ DMRG(12,28)-CASPT2,⁹⁷ theoretical best estimate (TBE),¹⁰⁰ and revised experiment.¹⁰⁰ As can be seen from Fig. 4, the present SDSPT2s and NEVPT2s PECs are very close to each other and are notably better than those by DMRG(12,22)-SC-NEVPT2⁹⁶ and DMRG(12,28)-CASPT2.⁹⁷ In particular, our SDSPT2s and NEVPT2s PECs are consistent with the latest TBE and revised experimental results¹⁰⁰ in the region between 2.0 and 2.4 Å, where the DMRG(12,22)-SC-NEVPT2 PEC exhibits a plateau.⁹⁶ The good quality of our SDSPT2s and NEVPT2s PECs is supported by the proximity and parallelity of the variational energies of iCISCF(12,22) and reduced space \tilde{P} , with the nonparallelity of their differences being only 0.22 mE_h for the whole interatomic distances (see Table S5 in the Supporting Information). Moreover, the weights of the CSFs of \tilde{P} are all more than 99% of those of iCISCF(12,22). As an additional indicator, the size-consistent errors of both SDSPT2s and NEVPT2s are less than 0.5 kcal/mol.

The spectroscopic constants of Cr₂, which were obtained by fitting the PEC between 1.55 and 1.8 Å, are given in Table 13. They are in fairly good agreement with the previous⁹⁶⁻⁹⁸ and experimental^{92,93,95} results.

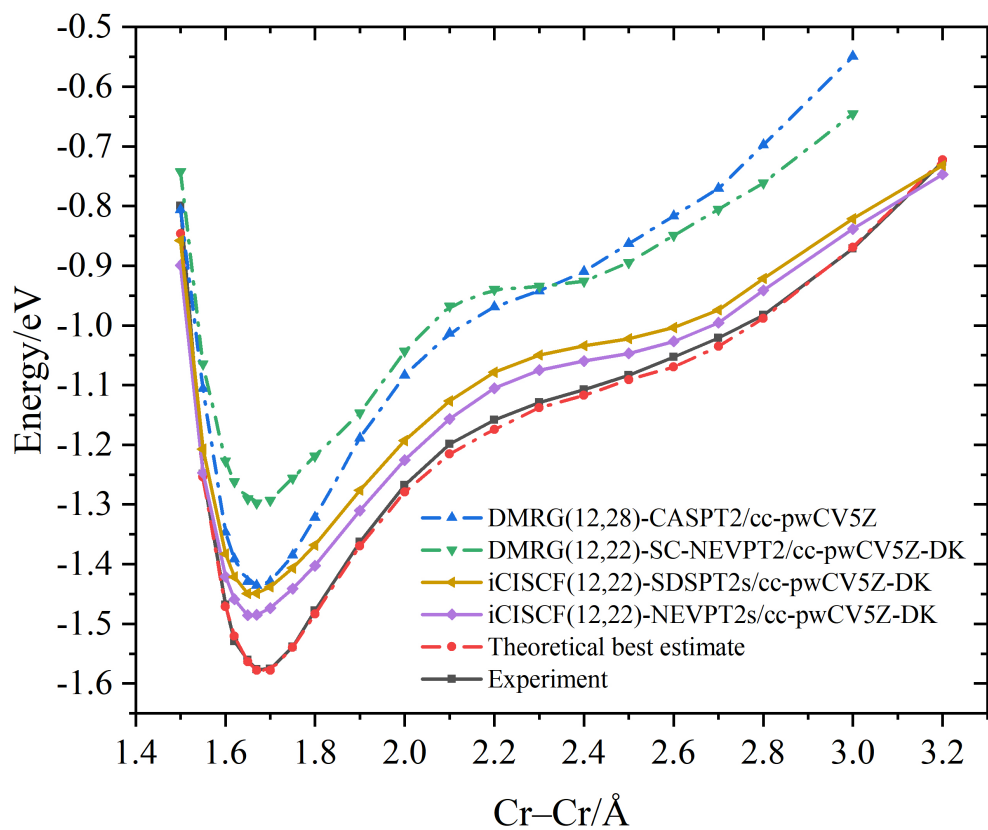


Figure 4: Potential energy curves of Cr_2 computed by iCISCF(12,22)-SDSPT2s/NEVPT2s [$C_{\min} = 10^{-4}$, $P_{\min} = 10^{-3}$, $Q_{\min} = 10^{-5}$, DVD], to compare with those by DMRG(12,22)-SC-NEVPT2,⁹⁶ DMRG(12,28)-CASPT2,⁹⁷ theoretical best estimate (TBE),¹⁰⁰ and revised experiment.¹⁰⁰

Table 13: Spectroscopic constants of Cr₂ by various MR methods

	R_e (Å)	D_e (eV)	ω_e (cm ⁻¹)
DMRG(12,28)-CASPT2/cc-pwCV5Z ^a	1.681	1.610	470
DMRG(12,22)-SC-NEVPT2/CBS ^b	1.655	1.435	469
iCISCF(12,22)-NEVPT2s/cc-pwCV5Z-DK ^c	1.658	1.486	469
iCISCF(12,22)-SDSPT2s/cc-pwCV5Z-DK ^c	1.659	1.449	462
DMRG(12,42)-ec-MRCISD+Q/ANO-RCC-VQZP ^d	1.71	1.62	479
Theoretical best estimate ^e	1.685	1.58±0.02	495
Experiment	1.679 ^f	1.47(5) ^g 1.56±0.06 ^h	481 ^g

^a Ref. 97; ^b Ref. 96; ^c This work; ^d Ref. 98; ^e Ref. 100; ^f Ref. 92; ^g Ref. 93; ^h Ref. 95.

4.5 [Cu₂O₂]²⁺ core

As a bi-copper system to activate O₂, [Cu₂O₂]²⁺ has been a popular model for validating quantum chemical methods. The isomerization energy between the bis(μ -oxo) ($F = 0.0$) and μ - η^2 : η^2 -peroxo ($F = 1.0$) isomers has been studied extensively by various approaches.^{37,81,102–106} To compare with the previous results by DMRG-SC-CTSD¹⁰⁴ and stochastic SC-NEVPT2 (SC-NEVPT2(s)),⁸¹ the same active space CAS(28,32) consisting of Cu $3d4d$ and O $2p3p$ was employed here, in conjunction with the ANO-RCC-VQZP basis sets^{107,108} and D_{2h} symmetry. The cartesian coordinates of different [Cu₂O₂]²⁺ structures were taken from Ref. 102 (see also Table S6 in the Supporting Information). The relative energies calculated by iCISCF(28,32)-NEVPT2s/SDSPT2s are presented in Table 14. The iCISCF(28,32) results show a shallow well at $F = 0.8$, indicating that accounting only for static correlation is insufficient. The NEVPT2s and SDSPT2s calculations yield nearly identical results, which are higher by 4 kcal/mol than those by SC-NEVPT2(s)⁸¹ for the structures between $F = 0.4$ to $F=0.8$. It turns out that such discrepancy stems from the different assemblies of the SDSPT2s/NEVPT2s and SC-NEVPT2(s) energies, $E_k^{(0)} + E_k^{(2)}$ vs. $\tilde{E}_k^{(0)} + E_k^{(2)}$. If the latter⁸¹ is also used in SDSPT2s/NEVPT2s, the discrepancy of 4 kcal/mol disappears (see values in brackets in Table 14), and the results become even

closer to those by DMRG-SC-CTSD¹⁰⁴ and especially to those by Ph-AFQMC (phaseless auxiliary field quantum Monte Carlo),¹⁰⁶ see Fig. 5. However, the error compensations between $\tilde{E}_k^{(0)}$ (positive error) and $E_k^{(2)}$ (negative error) does not hold in general. For instance, with this combination, the SDSPT2s dissociation energy of Cr₂ is only 1.11 eV, which is much smaller than that (1.45 eV) reported in Table 13.

Table 14: Energies (in kcal/mol) of [Cu₂O₂]²⁺ relative to μ - η^2 : η^2 -peroxo ($F = 1.0$)

Method	$F=0.0$	$F=0.2$	$F=0.4$	$F=0.6$	$F=0.8$	$F=1.0$
iCISCF ^{a,b}	18.5	11.1	5.6	1.1	-1.3	0.0
NEVPT2 _s ^{a,b,c}	40.9 [41.6]	35.4 [34.2]	30.5 [27.4]	23.9 [19.0]	13.1 [10.8]	0.0 [0.0]
SDSPT2 _s ^{a,b,c}	40.6 [41.4]	35.1 [33.8]	30.2 [27.1]	23.6 [18.8]	12.7 [10.3]	0.0 [0.0]
SC-NEVPT2(s) ^{a,d}	41.3(8)	33.5(9)	26.3(9)	19.9(8)	9.3(9)	0.0
DMRG-SC-CTSD ^{a,e}	37.4	29.0	22.0	14.4	6.1	0.0
Ph-AFQMC ^f	42.0	32.7	25.3	15.4	6.3	0.0

^a Active space (28e, 32o); ^b $C_{\min} = 10^{-4}$; ^c $P_{\min} = 10^{-3}$, $Q_{\min} = 10^{-5}$, DVD; values in brackets were derived from $\tilde{E}_k^{(0)} + E_k^{(2)}$; ^d Ref. 81; ^e Ref. 104; ^f adapted from Ref. 106 (52e results).

4.6 Cobalt Tropocoronand Complex

Transition metal (TM) tropocoronand (TC) nitrosyl complexes, [TM(TC- n,n)(NO)], have unusual geometric and electronic structures as function of the number of the alkylidene linkers. As one of the simplest representatives, the cobalt nitrosyl complex [Co(TC-3,3)(NO)] (see Fig. S2 in the Supporting Information) has been investigated both experimentally^{109,110} and theoretically.^{110,111} The early assignment¹⁰⁹ of its ground state to be paramagnetic (which is different from its homologues with larger n) was disapproved by a later density functional theory (DFT) and experimental study,¹¹⁰ which shows that the ground state of [Co(TC-3,3)(NO)] is diamagnetic. Interestingly, two distinct triplet states, denoted as T_1 and T_2 , have been obtained by DFT optimizations¹¹⁰ (see Tables S7–S9 in the Supporting Information for their cartesian coordinates). While the DFT reassignment of the ground state of [Co(TC-3,3)(NO)] was confirmed by subsequent DMRG(22,22)-SC-NEVPT2 calculations,¹¹¹ the underlying spin coupling mechanisms for the triplet states

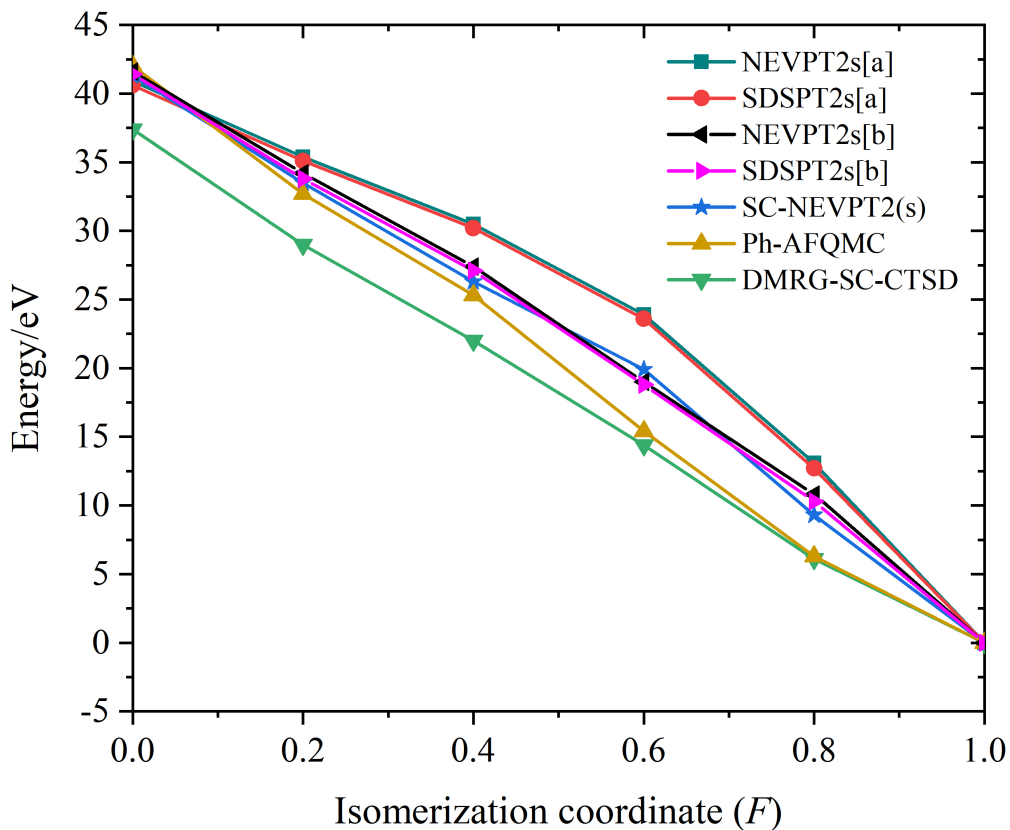


Figure 5: Relative energies of $[\text{Cu}_2\text{O}_2]^{2+}$ isomers by iCISCF(28,32)-SDSPT2s/NEVPT2s, to compare with those by HCISCF(28,32)-SC-NEVPT2(s),⁸¹ DMRG(28,32)-SC-CTSD,¹⁰⁴ and Ph-AFQMC (52e results).¹⁰⁶ SDSPT2s[a]/NEVPT2s[a] and SDSPT2s[b]/NEVPT2s[b] were derived from $E_k^{(0)} + E_k^{(2)}$ and $\tilde{E}_k^{(0)} + E_k^{(2)}$, respectively.

were interpreted differently. Therefore, we decided to carry out iCISCF(22,22)-SDSPT2s calculations with the def2-TZVP⁸⁸ and corresponding auxiliary basis sets for the RI approximation.⁸⁹ The active orbitals include five Co $3d$ and four Co $4d$, one σ ligand orbital (denoted as $\sigma_{3d_{xy}}$), four π and four π^* of TC-3,3, two π and two π^* of NO (see Figs. S3 to S6 in the Supporting Information for the converged active orbitals for the S_0 , T_1 , and T_2 states, respectively). It is first seen from Table 15 that the present iCISCF excitation energy (20.7 kcal/mol) for the T_1 state differs dramatically from that (38.6 kcal/mol) by DMRG-SCF,¹¹¹ which indicates strongly that the two SCF calculations did not converge to the same solution. To verify our results, we repeated the iCISCF(22,22) calculations for two triplet states (at the T_1 structure) but optimized only the second root (i.e., the weights for the first and second roots were set to zero and one, respectively). The excitation energy of the so-obtained second root is 38.1 (or 38.8) kcal/mol if the rotations between active orbitals were included (or not). Therefore, it can be concluded that the DMRG-SCF calculations¹¹¹ missed the energetically lower root. Consequently, the near-degeneracy between the T_1 and T_2 states (the lowest triplet states at two different structures¹¹⁰) revealed by the DMRG(22,22)-SC-NEVPT2 calculations¹¹¹ is spurious. They are actually separated by 20 kcal/mol.

It can be seen from Table 16 that the ground state of [Co(TC-3,3)(NO)] features a closed-shell configuration $3d^6\pi_{3d_2}^2$ but mixed with an anti-ferromagnetically coupled pair of half-spins at $3d^7$ ($S = 1/2$) and NO radical. This is in line with the DMRG-SCF assignment¹¹¹ and also supports the DFT calculations.¹¹⁰ The T_2 state is dominated by the ferromagnetic coupling between the half-spins at $3d^7$ and NO radical. In contrast, the two triplet states ($1T_1$ and $2T_2$) at the T_1 structure involve more complicated spin couplings, although both can be characterized as a mixture of motifs $3d^7\text{NO}$ and $3d^8\text{NO}^+$. Neither of the two is in line with the DMRG-SCF result, as can be seen from Fig. 6. Therefore, the

DMRG-SCF calculations should be repeated for these states.

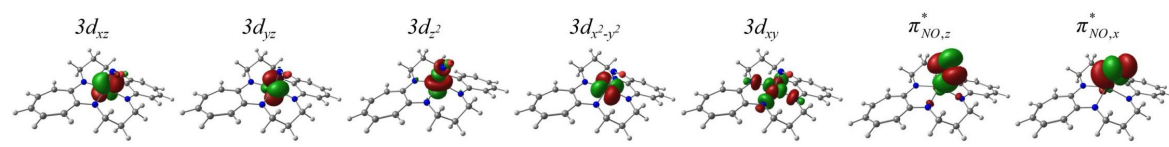
Table 15: Singlet-triplet energy gaps (in kcal/mol) of [Co(TC-3,3)(NO)]

State ^a	iCISCF ^b	SDSPT2s ^b	MS-NEVPT2s ^b	DMRG-SCF ^c	DMRG-SC-NEVPT2 ^c
$1T_1$	20.7	19.9 (14.7)	19.7 (14.5)	–	–
$2T_1$	38.1	39.6 (34.1)	39.6 (34.1)	38.6	35.0
T_2	29.7	40.1 (35.1)	40.3 (35.3)	29.6	36.1

^a $1T_1$ and $2T_1$ are the lowest two triplet states at the T_1 structure and T_2 the lowest triplet state at the T_2 structure.¹¹⁰

^b (22e, 22o), $C_{\min} = 10^{-4}$, $P_{\min} = 10^{-3}$, $Q_{\min} = 10^{-5}$, DVD; values in parentheses were derived from $\tilde{E}_k^{(0)} + E_k^{(2)}$.

^c Ref. 111, where $2T_1$ was regarded as $1T_1$.



	$3d_{xz}$	$3d_{yz}$	$3d_{z^2}$	$3d_{x^2-y^2}$	$3d_{xy}$	$\pi_{NO,z}^*$	$\pi_{NO,x}^*$
S_0	1.88 (1.90)	1.97 (1.96)	1.62 (1.77)	1.98 (1.98)	0.05 (0.04)	0.40 (0.25)	0.18 (0.14)
$1T_1$	1.66	1.48	1.00	1.97	1.01	0.56	0.39
$2T_1$	1.63 (1.91)	1.47 (1.54)	1.95 (1.00)	1.03 (1.98)	1.02 (1.00)	0.55 (0.48)	0.41 (0.15)
T_2	1.96 (1.95)	1.97 (1.97)	1.00 (1.00)	1.98 (1.98)	0.04 (0.04)	1.03 (1.03)	0.11 (0.10)

Figure 6: Natural orbital occupation numbers of key active orbitals of the S_0 , $1T_1$, $2T_1$, and T_2 states of [Co(TC-3,3)(NO)]. The $3d_{z^2}$ and $\pi_{NO,z}^*$ orbitals of S_0 are better characterized as π bonding ($\pi_{3d_{z^2}}$) and anti-bonding ($\pi_{3d_{z^2}}^*$) hybrids between $3d_{z^2}$ and $\pi_{NO,z}^*$ (see Fig. S3 in the Supporting Information). Values in parentheses were obtained by DMRG-SCF,¹¹¹ where $2T_1$ was regarded as $1T_1$.

Table 16: Leading configurations of the S_0 , $1T_1$, $2T_1$, and T_2 states of [Co(TC-3,3)(NO)] by iCISCF(22,22)/def2-TZVP with $C_{\min} = 10^{-4}$

State ^a	CSF ^b	Weight (%)	Character of Co	Character of NO
S_0	2222000	55.6	$3d^6 \pi_{3d_{z^2}}^2$ ($S = 0$)	
$1T_1$	2uu2ud0	24.9	$3d^7$ ($S = 3/2$)	NO ($S = 1/2$)
	u2u2u0d	11.5	$3d^7$ ($S = 3/2$)	NO ($S = 1/2$)
	2du2uu0	12.9	$3d^7$ ($S = 1/2$)	NO ($S = 1/2$)
	d2u2u0u	7.3	$3d^7$ ($S = 1/2$)	NO ($S = 1/2$)
	u2d2u0u	3.3	$3d^7$ ($S = 1/2$)	NO ($S = 1/2$)
	22u2u00	18.7	$3d^8$ ($S = 1$)	NO ⁺ ($S = 0$)
	$2T_1$	2u2uud0	19.4	$3d^7$ ($S = 3/2$)
u22uu0d		12.2	$3d^7$ ($S = 3/2$)	NO ($S = 1/2$)
2d2uuu0		10.5	$3d^7$ ($S = 1/2$)	NO ($S = 1/2$)
d22uu0u		6.6	$3d^7$ ($S = 1/2$)	NO ($S = 1/2$)
2u2duu0		6.4	$3d^7$ ($S = 1/2$)	NO ($S = 1/2$)
u22du0u		4.2	$3d^7$ ($S = 1/2$)	NO ($S = 1/2$)
222uu00		16.8	$3d^8$ ($S = 1$)	NO ⁺ ($S = 0$)
T_2	22u20u0	80.4	$3d^7$ ($S = 1/2$)	NO ($S = 1/2$)

^a $1T_1$ and $2T_1$ are the lowest two triplet states at the T_1 structure and T_2 the lowest triplet state at the T_2 structure.¹¹⁰

^b Sequences of active orbitals for S_0 and other states are $\text{Co}3d_{xz}$, $\text{Co}3d_{yz}$, $\pi_{3d_{z^2}}$, $\text{Co}3d_{x^2-y^2}$, $\text{Co}3d_{xy}$, $\pi_{3d_{z^2}}^*$, $\pi_{\text{NO},x}^*$ [$\pi_{3d_{z^2}} : \text{Co}3d_{z^2}$ (24.4%) and $\pi_{\text{NO},z}^*$ (74.3%); $\pi_{3d_{z^2}}^* : \text{Co}3d_{z^2}$ (75.4%) and $\pi_{\text{NO},z}^*$ (22.5%)] and $\text{Co}3d_{xz}$, $\text{Co}3d_{yz}$, $\text{Co}3d_{z^2}$, $\text{Co}3d_{x^2-y^2}$, $\text{Co}3d_{xy}$, $\pi_{\text{NO},z}^*$, $\pi_{\text{NO},x}^*$, respectively (see Figs. S3 to S6 in the Supporting Information); u: spin up; d: spin down.

5 Conclusions and outlook

It has been shown that both the computational cost and memory requirement of CASSCF-based SDSPT2 (and MS-NEVPT2) can be reduced substantially by virtue of configuration selection, without sacrificing the accuracy. This has been achieved by extending the highly efficient HPS-GUGA to incomplete reference spaces. Once the reduced sub-DRTs have been constructed, all matrix elements over internally contracted configurations can be evaluated in terms of DRT loops, precisely the same as in the case of a CAS reference. Further combined with an integral-based prescreening of batches of those double excitations involving three active orbitals, the resulting SDSPT2s (SDSPT2 with selection) can be applied to challenging systems that cannot be handled otherwise, as evidenced by sev-

eral examples presented here. Both SDSCI and ic-MRCISD can be simplified in the same way. However, the full potential of the reduced sub-DRT approach remains to be further explored. For instance, the prescreening of the CI subspaces other than $\bar{D}V$ and $\bar{V}D$ has not yet been pursued. To this end, we will investigate the possibility of first constructing reduced oCFG (instead of CSF) sub-DRTs, where the upper bounds⁵⁶ of the Hamiltonian matrix elements over oCFGs can be employed to eliminate unimportant excited oCFGs. The resulting oCFG sub-DRTs can then be stretched to the CSF ones. Work along this direction is being carried out at our laboratory.

Acknowledgements

This work was supported by National Natural Science Foundation of China (Grant Nos. 22273071, 22273052 and 22373057) and Mount Tai Climbing Program of Shandong Province.

Supporting Information

Brief description of GUGA distinct row table; cartesian coordinates of $\text{Fe}^{\text{II}}\text{L}_2$, $[\text{Cu}_2\text{O}_2]^{2+}$, and $[\text{Co}(\text{TC-3,3})(\text{NO})]$; active orbitals of $\text{Fe}^{\text{II}}\text{L}_2$ and $[\text{Co}(\text{TC-3,3})(\text{NO})]$; energies of Cr_2 at different interatomic distances.

Conflicts of interest

There are no conflicts to declare.

References

- (1) Liu, W.; Hoffmann, M. R. iCI: Iterative CI toward full CI. *J. Chem. Theory Comput.* **2016**, *12*, 1169–1178, (E)**12**, 3000 (2016).
- (2) Andersson, K.; Malmqvist, P.-A.; Roos, B. O.; Sadlej, A. J.; Wolinski, K. Second-Order Perturbation Theory with a CASSCF Reference Function. *J. Phys. Chem.* **1990**, *94*, 5483–5488.
- (3) Andersson, K.; Malmqvist, P.-A.; Roos, B. O. Second-order perturbation theory with a complete active space self-consistent field reference function. *J. Chem. Phys.* **1992**, *96*, 1218–1226.
- (4) Nakano, H. Quasidegenerate perturbation theory with multiconfigurational self-consistent-field reference functions. *J. Chem. Phys.* **1993**, *99*, 7983–7992.
- (5) Angeli, C.; Cimiraglia, R.; Evangelisti, S.; Leininger, T.; Malrieu, J.-P. Introduction of n-electron valence states for multireference perturbation theory. *J. Chem. Phys.* **2001**, *114*, 10252–10264.
- (6) Angeli, C.; Cimiraglia, R.; Malrieu, J.-P. N-electron valence state perturbation theory: a fast implementation of the strongly contracted variant. *Chem. Phys. Lett.* **2001**, *350*, 297–305.
- (7) Finley, J.; Malmqvist, P.-A.; Roos, B. O.; Serrano-Andrés, L. The multi-state CASPT2 method. *Chem. Phys. Lett.* **1998**, *288*, 299–306.
- (8) Granovsky, A. A. *J. Chem. Phys.* **2011**, *134*, 214113.
- (9) Shiozaki, T.; Győrffy, W.; Celani, P.; Werner, H.-J. Communication: Extended multi-state complete active space second-order perturbation theory: Energy and nuclear gradients. *J. Chem. Phys.* **2011**, *135*, 081106.

- (10) Angeli, C.; Borini, S.; Cestari, M.; Cimiraglia, R. A quasidegenerate formulation of the second order n-electron valence state perturbation theory approach. *J. Chem. Phys.* **2004**, *121*, 4043–4049.
- (11) Gershgorn, Z.; Shavitt, I. An application of perturbation theory ideas in configuration interaction calculations. *Int. J. Quantum Chem.* **1968**, *2*, 751–759.
- (12) Davidson, E. R.; Murchie, L. E. M.; Day, S. J. The B_k method: Application to methylene. *J. Chem. Phys.* **1981**, *74*, 5491–5496.
- (13) Shavitt, I. The A_k and B_k approximate CI methods. Comment on a paper by Maynau and Heully. *Chem. Phys. Lett.* **1992**, *192*, 135–137.
- (14) Rawlings, D. C.; Davidson, E. R. The Rayleigh-Schrödinger B_k method applied to the lower electronic states of pyrrole. *Chem. Phys. Lett.* **1983**, *98*, 424–427.
- (15) Lei, Y.; Wang, Y.; Han, H.; Song, Q.; Suo, B.; Wen, Z. New implementation of the configuration-based multi-reference second order perturbation theory. *J. Chem. Phys.* **2012**, *137*, 144102.
- (16) Pathak, S.; Lang, L.; Neese, F. A dynamic correlation dressed complete active space method: Theory, implementation, and preliminary applications. *J. Chem. Phys.* **2017**, *147*.
- (17) Hoffmann, M. R. Canonical Van Vleck quasidegenerate perturbation theory with trigonometric variables. *J. Phys. Chem.* **1996**, *100*, 6125–6130.
- (18) Khait, Y. G.; Song, J.; Hoffmann, M. R. Explication and revision of generalized Van Vleck perturbation theory for molecular electronic structure. *J. Chem. Phys.* **2002**, *117*, 4133–4145.

- (19) Jiang, W.; Khait, Y. G.; Hoffmann, M. R. Configuration-Driven Unitary Group Approach for Generalized Van Vleck Variant Multireference Perturbation Theory. *J. Phys. Chem. A* **2009**, *113*, 4374–4380.
- (20) Mahapatra, U. S.; Datta, B.; Mukherjee, D. Molecular applications of a size-consistent state-specific multireference perturbation theory with relaxed model-space coefficients. *J. Phys. Chem. A* **1999**, *103*, 1822–1830.
- (21) Mahapatra, U. S.; Datta, B.; Mukherjee, D. Development of a size-consistent state-specific multireference perturbation theory with relaxed model-space coefficients. *Chem. Phys. Lett.* **1999**, *299*, 42–50.
- (22) P.Ghosh; Chattopadhyay, S.; Jana, D.; Mukherjee, D. State-specific Multi-reference Perturbation Theories with Relaxed Coefficients: Molecular Applications. *Int. J. Mol. Sci.* **2002**, *3*, 733–754.
- (23) Mao, S.; L. Cheng, W. L.; Mukherjee, D. A spin-adapted size-extensive state-specific multi-reference perturbation theory. I. Formal developments. *J. Chem. Phys.* **2012**, *136*, 024105.
- (24) Mao, S.; Cheng, L.; Liu, W.; Mukherjee, D. A spin-adapted size-extensive state-specific multi-reference perturbation theory with various partitioning schemes. II. Molecular applications. *J. Chem. Phys.* **2012**, *136*, 024106.
- (25) Li, C.; Evangelista, F. A. Multireference Driven Similarity Renormalization Group: A Second-Order Perturbative Analysis. *J. Chem. Theory Comput.* **2015**, *11*, 2097–2108.
- (26) Li, C.; Evangelista, F. A. Driven similarity renormalization group for excited states: A state-averaged perturbation theory. *J. Chem. Phys.* **2018**, *148*, 124106.
- (27) Werner, H. J.; Reinsch, E. A. The self-consistent electron pairs method for multiconfiguration reference state functions. *J. Chem. Phys.* **1982**, *76*, 3144–3156.

- (28) Knowles, P. J.; Werner, H.-J. An efficient method for the evaluation of coupling coefficients in configuration interaction calculations. *Chem. Phys. Lett.* **1988**, *145*, 514–522.
- (29) Werner, H. J. An efficient internally contracted multiconfiguration reference configuration-interaction method. *J. Chem. Phys.* **1988**, *89*, 5803–5814.
- (30) Knowles, P. J.; Werner, H. J. Internally contracted multiconfiguration-reference configuration-interaction calculations for excited-states. *Theor. Chim. Acta* **1992**, *84*, 95–103.
- (31) Shamasundar, K. R.; Knizia, G.; Werner, H. J. A new internally contracted multi-reference configuration interaction method. *J. Chem. Phys.* **2011**, *135*, 054101.
- (32) Wang, Y.; Zhai, G.; Suo, B.; Gan, Z.; Wen, Z. Hole-particle correspondence in CI calculations. *Chem. Phys. Lett.* **2003**, *375*, 134–140.
- (33) Wang, Y.; Han, H.; Lei, Y.; Suo, B.; Zhu, H.; Song, Q.; Wen, Z. New schemes for internally contracted multi-reference configuration interaction. *J. Chem. Phys.* **2014**, *141*, 164114.
- (34) Suo, B.; Lei, Y.; Han, H.; Wang, Y. Development of Xi'an-CI package—applying the hole-particle symmetry in multi-reference electronic correlation calculations. *Mol. Phys.* **2018**, *116*, 1051–1064.
- (35) Sivalingam, K.; Krupicka, M.; Auer, A. A.; Neese, F. Comparison of fully internally and strongly contracted multireference configuration interaction procedures. *J. Chem. Phys.* **2016**, *145*, 054104.
- (36) Song, Q.; Liu, B.; Wu, J.; Zou, W.; Wang, Y.; Suo, B.; Lei, Y. GUGA-based MRCI approach with core-valence separation approximation (CVS) for the calculation of the core-excited states of molecules. *J. Chem. Phys.* **2024**, *160*, 094114.

- (37) Cheng, Y.; Ma, H. Renormalized-Residue-Based Multireference Configuration Interaction Method for Strongly Correlated Systems. *J. Chem. Theory Comput.* **2024**, *20*, 1988–2009.
- (38) Sherrill, C. D.; Schaefer III, H. F. The configuration interaction method: Advances in highly correlated approaches. *Adv. Quantum Chem.* **1999**, *34*, 143–269.
- (39) Szalay, P. G.; Muller, T.; Gidofalvi, G.; Lischka, H.; Shepard, R. Multiconfiguration self-consistent field and multireference configuration interaction methods and applications. *Chem. Rev.* **2012**, *112*, 108–181.
- (40) Mahapatra, U. S.; Datta, B.; Bandyopadhyay, B.; Mukherjee, D. State-specific multi-reference coupled cluster formulations: Two paradigms. *Adv. Quantum Chem.* **1998**, *30*, 163–193.
- (41) Hanrath, M. An exponential multireference wave-function Ansatz. *J. Chem. Phys.* **2005**, *123*, 084102.
- (42) Evangelista, F. A.; Gauss, J. An orbital-invariant internally contracted multireference coupled cluster approach. *J. Chem. Phys.* **2011**, *134*, 114102.
- (43) Hanauer, M.; Köhn, A. Pilot applications of internally contracted multireference coupled cluster theory, and how to choose the cluster operator properly. *J. Chem. Phys.* **2011**, *134*, 204111.
- (44) Hanauer, M.; Köhn, A. Communication: Restoring full size extensivity in internally contracted multireference coupled cluster theory. *J. Chem. Phys.* **2012**, *137*, 131103.
- (45) Sinha, D.; Maitra, R.; Mukherjee, D. Generalized antisymmetric ordered products, generalized normal ordered products, ordered and ordinary cumulants and their use in many electron correlation problem. *Comput. Theor. Chem.* **2013**, *1003*, 62–70.

- (46) Hanauer, M.; Köhn, A. Communication: Restoring full size extensivity in internally contracted multireference coupled cluster theory. *J. Chem. Phys.* **2012**, *137*.
- (47) Köhn, A.; Hanauer, M.; Mück, L. A.; Jagau, T.-C.; Gauss, J. State-specific multireference coupled-cluster theory. *WIREs: Comput. Mol. Sci.* **2013**, *3*, 176–197.
- (48) Hubač, I.; Neogrády, P. Size-consistent brillouin-wigner perturbation-theory with an exponentially parametrized wave-function - brillouin-wigner coupled-cluster theory. *Phys. Rev. A* **1994**, *50*, 4558–4564.
- (49) Masik, J.; P., I. H.; Mach Single-root multireference Brillouin-Wigner coupled-cluster theory: Applicability to the F₂ molecule. *J. Chem. Phys.* **1998**, *108*, 6571–6579.
- (50) Mahapatra, U. S.; B. Datta, B. B.; Mukherjee, D. A state-specific multi-reference coupled cluster formalism with molecular applications. *Mol. Phys.* **1998**, *94*, 157–171.
- (51) Mahapatra, U. S.; Datta, B.; Mukherjee, D. A size-consistent state-specific multireference coupled cluster theory: Formal developments and molecular applications. *J. Chem. Phys.* **1999**, *110*, 6171–6188.
- (52) Malrieu, J. P. Proposal of multi-root multi-reference coupled cluster formalisms. *Mol. Phys.* **2013**, *111*, 2451–2462.
- (53) Lyakh, D. I.; Musiaz, M.; Lotrich, V. F.; Bartlett, R. J. Multireference nature of chemistry: The coupled-cluster view. *Chem. Rev.* **2012**, *112*, 182–243.
- (54) Liu, W.; Hoffmann, M. R. SDS: the 'static-dynamic-static' framework for strongly correlated electrons. *Theor. Chem. Acc.* **2014**, *133*, 1481.
- (55) Lei, Y.; Liu, W.; Hoffmann, M. R. Further development of SDSPT2 for strongly correlated electrons. *Mol. Phys.* **2017**, *115*, 2696–2707.
- (56) Zhang, N.; Liu, W.; Hoffmann, M. R. Iterative Configuration Interaction with Selection. *J. Chem. Theory Comput.* **2020**, *16*, 2296–2316.

- (57) Zhang, N.; Liu, W.; Hoffmann, M. R. Further Development of iCIPT2 for Strongly Correlated Electrons. *J. Chem. Theory Comput.* **2021**, *17*, 949–964.
- (58) Liu, W. Perspective: Simultaneous treatment of relativity, correlation, and QED. *WIREs Comput. Mol. Sci.* **2023**, *13*, e1652.
- (59) Song, Y.; Guo, Y.; Lei, Y.; Zhang, N.; Liu, W. The static-dynamic-static family of methods for strongly correlated electrons: Methodology and benchmarking. *Top. Curr. Chem.* **2021**, *379*, 43.
- (60) Song, Y.; Zhang, N.; Lei, Y.; Guo, Y.; Liu, W. QUEST#4X: an extension of QUEST#4 for benchmarking multireference wavefunction methods. *arXiv preprint* **2024**, arXiv:2409.00302.
- (61) Li, J.; Wu, C.; Lei, Y.; Liu, W. Tuning Catalyst-Free Photocontrolled Polymerization by Substitution: A Quantitative and Qualitative Interpretation. *J. Phys. Chem. Lett.* **2022**, *13*, 3290–3296.
- (62) Wang, X.; Wu, C.; Wang, Z.; Liu, W. When do tripdoublet states fluoresce? A theoretical study of copper (II) porphyrin. *Frontiers in Chemistry* **2023**, *11*, 1259016.
- (63) Wang, H.; Yang, T.; Li, Y.; Yu, L.; Lei, Y.; Zhu, C. Nonadiabatic molecular dynamics simulations for ultrafast photo-induced ring-opening and isomerization reactions of 2, 2-diphenyl-2 H-chromene. *Phys. Chem. Chem. Phys.* **2023**, *25*, 31363–31373.
- (64) Phung, Q. M.; Nam, H. N.; Saitow, M. Unraveling the Spin-State Energetics of FeN₄ Complexes with Ab Initio Methods. *J. Phys. Chem. A* **2023**, *127*, 7544–7556.
- (65) Eriksen, J. J.; Anderson, T. A.; Deustua, J. E.; Ghanem, K.; Hait, D.; Hoffmann, M. R.; Lee, S.; Levine, D. S.; Magoulas, I.; Shen, J.; Tubman, N. M.; Whaley, K. B.; Xu, E.; Yao, Y.; Zhang, N.; Alavi, A.; Chan, G. K.-L.; Head-Gordon, M.; Liu, W.; Piecuch, P.;

- Sharma, S.; Ten-no, S. L.; Umrigar, C. J.; Gauss, J. The Ground State Electronic Energy of Benzene. *J. Phys. Chem. Lett.* **2020**, *11*, 8922–8929.
- (66) Guo, Y.; Zhang, N.; Lei, Y.; Liu, W. iCISCF: An Iterative Configuration Interaction-Based Multiconfigurational Self-Consistent Field Theory for Large Active Spaces. *Journal of Chemical Theory and Computation* **2021**, *17*, 7545–7561.
- (67) Staroverov, V. N.; Davidson, E. R. The reduced model space method in multireference second-order perturbation theory. *Chem. Phys. Lett.* **1998**, *296*, 435–444.
- (68) Celani, P.; Werner, H.-J. Multireference perturbation theory for large restricted and selected active space reference wave functions. *J. Chem. Phys.* **2000**, *112*, 5546–5557.
- (69) Nakano, H.; Uchiyama, R.; Hirao, K. Quasi-degenerate perturbation theory with general multiconfiguration self-consistent field reference functions. *J. Comput. Chem.* **2002**, *23*, 1166–1175.
- (70) Grimme, S.; Waletzke, M. Multi-reference Møller–Plesset theory: computational strategies for large molecules. *Phys. Chem. Chem. Phys.* **2000**, *2*, 2075–2081.
- (71) Shavitt, I. Graph theoretical concepts for the unitary group approach to the many-electron correlation problem. *Int. J. Quantum Chem.* **1977**, *S11*, 131–149.
- (72) Dylla, K. G. The choice of a zeroth-order Hamiltonian for second-order perturbation theory with a complete active space self-consistent-field reference function. *J. Chem. Phys.* **1995**, *102*, 4909–4918.
- (73) Pople, J. A.; Seeger, R.; Krishnan, R. Variational configuration interaction methods and comparison with perturbation theory. *Int. J. Quantum Chem.* **1977**, *12*, 149–163.
- (74) Epstein, P. S. The stark effect from the point of view of Schroedinger's quantum theory. *Phys. Rev.* **1926**, *28*, 695.

- (75) Nesbet, R. K. Configuration interaction in orbital theories. *Proc. Roy. Soc. of London. Series A. Math. Phys. Sci.* **1955**, 230, 312–321.
- (76) Chilkuri, V. G.; Neese, F. Comparison of many-particle representations for selected-CI I: A tree based approach. *J. Comput. Chem.* **2021**, 42, 982–1005.
- (77) Helgaker, T.; Jorgensen, P.; Olsen, J. *Molecular Electronic-Structure Theory*; John Wiley & Sons, 2014.
- (78) Li, Z.; Xiao, Y.; Liu, W. On the spin separation of algebraic two-component relativistic Hamiltonians. *J. Chem. Phys.* **2012**, 137, 154114.
- (79) Li, Z.; Xiao, Y.; Liu, W. On the spin separation of algebraic two-component relativistic Hamiltonians: Molecular properties. *J. Chem. Phys.* **2014**, 141, 054111.
- (80) Lei, Y.; Suo, B.; Liu, W. iCAS: Imposed Automatic Selection and Localization of Complete Active Spaces. *J. Chem. Theory Comput.* **2021**, 17, 4846–4859.
- (81) Blunt, N. S.; Mahajan, A.; Sharma, S. Efficient multireference perturbation theory without high-order reduced density matrices. *J. Chem. Phys.* **2020**, 153, 164120.
- (82) Liu, W.; Hong, G.; Dai, D.; Li, L.; Dolg, M. The Beijing 4-component density functional theory program package (BDF) and its application to EuO, EuS, YbO and YbS. *Theor. Chem. Acc.* **1997**, 96, 75–83.
- (83) Liu, W.; Wang, F.; Li, L. *J. Theor. Comput. Chem.* **2003**, 2, 257–272.
- (84) Liu, W.; Wang, F.; Li, L. In *Recent Advances in Relativistic Molecular Theory*; Hirao, K., Ishikawa, Y., Eds.; World Scientific: Singapore, 2004; pp 257–282.
- (85) Zhang, Y.; Suo, B.; Wang, Z.; Zhang, N.; Li, Z.; Lei, Y.; Zou, W.; Gao, J.; Peng, D.; Pu, Z.; Xiao, Y.; Sun, Q.; Wang, F.; Ma, Y.; Wang, X.; Guo, Y.; Liu, W. BDF: A relativistic electronic structure program package. *J. Chem. Phys.* **2020**, 152, 064113.

- (86) Radoń, M. Spin-State Energetics of Heme-Related Models from DFT and Coupled Cluster Calculations. *J. Chem. Theory Comput.* **2014**, *10*, 2306–2321.
- (87) Pierloot, K.; Phung, Q. M.; Domingo, A. Spin State Energetics in First-Row Transition Metal Complexes: Contribution of (3s3p) Correlation and Its Description by Second-Order Perturbation Theory. *J. Chem. Theory Comput.* **2017**, *13*, 537–553.
- (88) Weigend, F.; Ahlrichs, R. Balanced basis sets of split valence, triple zeta valence and quadruple zeta valence quality for H to Rn: Design and assessment of accuracy. *Phys. Chem. Chem. Phys.* **2005**, *7*, 3297–3305.
- (89) Weigend, F.; Häser, M.; Patzelt, H.; Ahlrichs, R. RI-MP2: optimized auxiliary basis sets and demonstration of efficiency. *Chem. Phys. Lett.* **1998**, *294*, 143–152.
- (90) Dunning, T. H. Gaussian basis sets for use in correlated molecular calculations. I. The atoms boron through neon and hydrogen. *J. Chem. Phys.* **1989**, *90*, 1007–1023.
- (91) Park, J. W. Second-Order Orbital Optimization with Large Active Spaces Using Adaptive Sampling Configuration Interaction (ASCI) and Its Application to Molecular Geometry Optimization. *J. Chem. Theory Comput.* **2021**, *17*, 1522–1534.
- (92) Bondybey, V.; English, J. Electronic structure and vibrational frequency of Cr₂. *Chem. Phys. Lett.* **1983**, *94*, 443–447.
- (93) Casey, S. M.; Leopold, D. G. Negative ion photoelectron spectroscopy of chromium dimer. *J. Phys. Chem.* **1993**, *97*, 816–830.
- (94) Bauschlicher, C. W.; Partridge, H. Cr₂ revisited. *Chem. Phys. Lett.* **1994**, *231*, 277–282.
- (95) Simard, B.; Lebeault-Dorget, M.-A.; Marijnissen, A.; ter Meulen, J. J. Photoionization spectroscopy of dichromium and dimolybdenum: Ionization potentials and bond energies. *J. Chem. Phys.* **1998**, *108*, 9668–9674.

- (96) Guo, S.; Watson, M. A.; Hu, W.; Sun, Q.; Chan, G. K.-L. N-Electron Valence State Perturbation Theory Based on a Density Matrix Renormalization Group Reference Function, with Applications to the Chromium Dimer and a Trimer Model of Poly(p-Phenylenevinylene). *J. Chem. Theory Comput.* **2016**, *12*, 1583–1591.
- (97) Kurashige, Y.; Yanai, T. Second-order perturbation theory with a density matrix renormalization group self-consistent field reference function: Theory and application to the study of chromium dimer. *J. Chem. Phys.* **2011**, *135*, 094104.
- (98) Luo, Z.; Ma, Y.; Wang, X.; Ma, H. Externally-Contracted Multireference Configuration Interaction Method Using a DMRG Reference Wave Function. *J. Chem. Theory Comput.* **2018**, *14*, 4747–4755.
- (99) Li, J.; Yao, Y.; Holmes, A. A.; Otten, M.; Sun, Q.; Sharma, S.; Umrigar, C. J. Accurate many-body electronic structure near the basis set limit: Application to the chromium dimer. *Phys. Rev. Res.* **2020**, *2*, 012015.
- (100) Larsson, H. R.; Zhai, H.; Umrigar, C. J.; Chan, G. K.-L. The Chromium Dimer: Closing a Chapter of Quantum Chemistry. *J. Am. Chem. Soc.* **2022**, *144*, 15932–15937.
- (101) Balabanov, N. B.; Peterson, K. A. Systematically convergent basis sets for transition metals. I. All-electron correlation consistent basis sets for the 3d elements Sc-Zn. *J. Chem. Phys.* **2005**, *123*, 064107.
- (102) Cramer, C. J.; Włoch, M.; Piecuch, P.; Puzzarini, C.; Gagliardi, L. Theoretical Models on the Cu₂O₂ Torture Track: Mechanistic Implications for Oxytyrosinase and Small-Molecule Analogues. *J. Phys. Chem. A* **2006**, *110*, 1991–2004.
- (103) Malmqvist, P.; Pierloot, K.; Shahi, A. R. M.; Cramer, C. J.; Gagliardi, L. The restricted active space followed by second-order perturbation theory method: Theory and application to the study of CuO₂ and Cu₂O₂ systems. *J. Chem. Phys.* **2008**, *128*, 204109.

- (104) Yanai, T.; Kurashige, Y.; Neuscamman, E.; Chan, G. K.-L. Multireference quantum chemistry through a joint density matrix renormalization group and canonical transformation theory. *J. Chem. Phys.* **2010**, *132*, 024105.
- (105) Phung, Q. M.; Wouters, S.; Pierloot, K. Cumulant Approximated Second-Order Perturbation Theory Based on the Density Matrix Renormalization Group for Transition Metal Complexes: A Benchmark Study. *J. Chem. Theory Comput.* **2016**, *12*, 4352–4361.
- (106) Landinez Borda, E. J.; Gomez, J.; Morales, M. A. Non-orthogonal multi-Slater determinant expansions in auxiliary field quantum Monte Carlo. *J. Chem. Phys.* **2019**, *150*, 074105.
- (107) Roos, B. O.; Lindh, R.; Malmqvist, P.-Å.; Veryazov, V.; Widmark, P.-O. Main Group Atoms and Dimers Studied with a New Relativistic ANO Basis Set. *J. Phys. Chem. A* **2004**, *108*, 2851–2858.
- (108) Roos, B. O.; Lindh, R.; Malmqvist, P.-Å.; Veryazov, V.; Widmark, P.-O. New Relativistic ANO Basis Sets for Transition Metal Atoms. *J. Phys. Chem. A* **2005**, *109*, 6575–6579.
- (109) Ellison, M. K.; Scheidt, W. R. Tilt/asymmetry in nitrosyl metalloporphyrin complexes: The cobalt case. *Inorg. Chem.* **1998**, *37*, 382–383.
- (110) Hopmann, K. H.; Conradie, J.; Tangen, E.; Tonzetich, Z. J.; Lippard, S. J.; Ghosh, A. Singlet-Triplet Gaps of Cobalt Nitrosyls: Insights from Tropocoronand Complexes. *Inorg. Chem.* **2015**, *54*, 7362–7367.
- (111) Freitag, L.; Knecht, S.; Angeli, C.; Reiher, M. Multireference Perturbation Theory with Cholesky Decomposition for the Density Matrix Renormalization Group. *J. Chem. Theory Comput.* **2017**, *13*, 451–459.